Published for SISSA by Springer

Received: *March 9, 2023*
Accepted: *May 17, 2023*
Published: *June 6, 2023*

Large primordial fluctuations in gravitational waves from phase transitions

Arushi Bodas and Raman Sundrum

Maryland Center for Fundamental Physics, Department of Physics, University of Maryland, College Park, MD 20742, U.S.A.

E-mail: arushib@terpmail.umd.edu, raman@umd.edu

Abstract: It is well-known that first-order phase transitions in the early universe can be a powerful source of observable stochastic gravitational wave backgrounds. Any such gravitational wave background must exhibit large-scale anisotropies *at least* as large as those seen in the CMB $\sim 10^{-5}$, providing a valuable new window onto the (inflationary) origins of primordial fluctuations. While significantly larger fractional anisotropies are possible (for example, in multi-field inflation) and would be easier to interpret, it has been argued that these can only be consistent with CMB bounds if the gravitational wave signal is correspondingly smaller. In this paper, we show that this argument, which relies on assuming radiation dominance of the very early universe, can be evaded if there is an era of early matter dominance of a certain robust type. This allows large gravitational wave anisotropies to be consistent with observable signals at proposed future gravitational wave detectors. Constraints from the CMB on large scales, as well as primordial black hole and mini-cluster formation on small scales, and secondary scalar-induced gravitational waves are all taken into account.

Keywords: Early Universe Particle Physics, Phase Transitions in the Early Universe

ArXiv ePrint: 2211.09301

https://doi.org/10.1007/JHEP06(2023)029

JHEP06(2023)029

Contents

1 Introduction

Well-motivated particle physics beyond the Standard Model (BSM) can readily undergo first-order phase transitions in the early universe, which can be powerful sources of observable stochastic gravitational wave backgrounds (GWB) (see [1, 2] for a review). For example, a critical temperature in the (multi-)TeV range would result in GWB in the frequency range of the LISA detector [3]. The frequency spectrum of a GWB would encode valuable information about the BSM dynamics. Complementary to the frequency spectrum, such a GWB would necessarily also exhibit large-scale anisotropies, analogous to those of the CMB. This was shown in ref. [4]. GWB anisotropies in other contexts have also been discussed in [5–11]. In the inflationary paradigm, these anisotropies would reflect quantum fluctuations in inflation-era fields, giving us an invaluable new window into their poorly understood dynamics. In particular, if there are multiple light fields during inflation, ref. [4] showed that the GWB anisotropies could have a significant isocurvature component, very different from the standard adiabatic perturbations of the CMB and Large Scale Structure (LSS). Refs. [12, 13] have explored the potential of such isocurvature GWB maps from phase transitions as a probe of early universe physics.

JHEP06(2023)029

The presence of isocurvature in GWB would imply the existence of another light quantum field during inflation. However, to be readily distinguished and interpreted the isocurvature should be larger than the CMB anisotropy. This is because any GWB would receive an irreducible contribution from the adiabatic perturbations through the gravitational Sachs-Wolfe effect $\sim 10^{-5}$ [9, 12, 14, 15]. Therefore, large fractional anisotropies $> 10^{-5}$ in the GWB would be ideal for revealing new inflationary physics.

For example, a well-motivated candidate for a light spectator field during inflation is an (unstable) axion-like particle (ALP) with an initial misalignment from its minimum (see [16, 17] for a review of ALPS). The overall level of anisotropy is then given by the ratio of the inflationary Hubble scale to the initial field misalignment. In high-scale inflation where the Hubble constant is taken to be $\sim 10^{-5}$ times the Planck scale [18], the ALP fluctuations are likely to be $\gg 10^{-5}$ if the ALP misalignment is constrained to being sub-Planckian. Also, if the Hubble constant during inflation can be inferred independently, through the detection of primordial tensor modes for example [19], then the measurement of GWB isocurvature would give us the initial misalignment of the ALP field. Therefore, large isocurvature GWB sourced by this ALP field would be an ideal target for gravitational wave experiments.

Unfortunately, there is a significant challenge for large GWB anisotropies to even be detectable. A distinct isocurvature GWB requires that there be two mostly decoupled sectors at the time of the phase transition: one sector with adiabatic perturbation reheated by the inflaton, and another undergoing the phase transition reheated by a separate light field, in our case an ALP. The phase-transitioning sector in such a case must be significantly subdominant at recombination to avoid its impact on the CMB, which is highly constrained from observations. In the case of standard radiation dominance in the early universe, this subdominance implies a strong suppression in the overall strength of the GWB signal [4], making detection of large anisotropies extremely difficult at upcoming or proposed detectors.

In this work, we will show that the trade-off between large fractional anisotropy and detectability of GW signals can be evaded if there is a period of early matter dominance (eMD)[1] in the cosmological history. In this scenario, the phase-transitioning sector can be dominant at the time of the phase transition, avoiding suppression in GW signal at its production time. A later stage of eMD in the adiabatic sector will dilute the phase-transitioning sector such that its contribution to CMB anisotropies is subdominant. It would necessarily also dilute the overall GWB, but we will show that this dilution is less severe. Importantly, the anisotropic component is left unsuppressed in absolute size, which brings a larger range of anisotropies within the sensitivity of upcoming detectors.

The paper is organized as follows. In section 2, we review the original model of isocurvature GWB from a phase transition from [4], in which the phase transition and adiabatic sectors of the very early universe are always radiation-dominated, prior to merging into a single sector via (late) particle decays. We re-examine why, with radiation dominance, consistency with CMB constraints predicts that large fractional anisotropies in the GWB must come at the expense of suppressed signal strength, both in the isotropic and anisotropic components. In section 3, we introduce our new eMD model and show how a large fractional anisotropy in the GWB is consistent with CMB constraints, along the lines sketched above.

[1] Early in this context means before Big Bang Nucleosynthesis.

JHEP06(2023)029

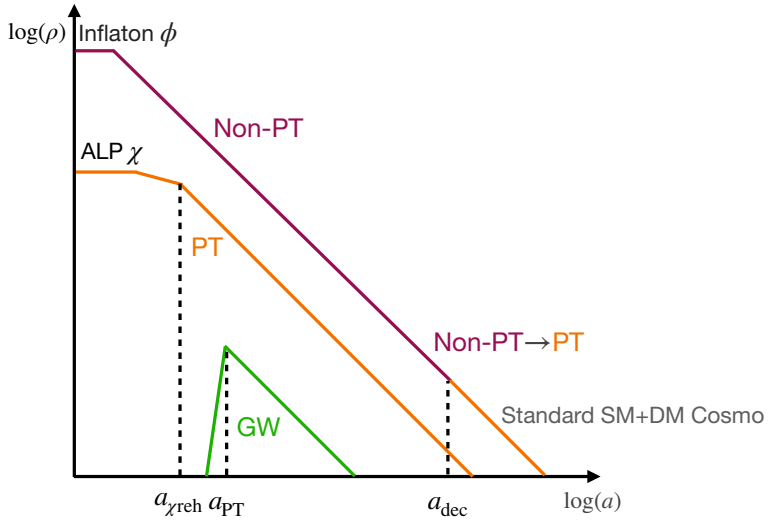

Figure 1. A schematic of the model discussed in section 2 showing energy densities in various sectors as a function of the scale factor (time). The decay products of both the inflaton and ALP χ are always radiation dominated in this model.

We also show that the eMD dilution of the GWB results in only a modest redshift of the GW frequency spectrum relative to the original model. In section 4, we consider the gravitational interactions between the phase transition and adiabatic sectors prior to their merging to see that they do no affect our conclusions in section 3 on large scales, but also to consider new constraints on small scales from primordial black hole production, small-scale structure formation, and scalar-induced gravitational wave production at second order. In section 5, we present plausible benchmarks in our model with different fractional GWB anisotropies and the associated isotropic and anisotropic signal strengths. We compare with the analogous benchmarks in the original radiation-dominated model to illustrate the significant gains in signal strength, in both the isotropic and anisotropic components. We conclude in section 6 with a short discussion of the significance of our results.

2 Isocurvature GWB in the radiation-dominated model

In this section, we review the model proposed in ref. [4] that produces isocurvature GWB. Consider an additional light scalar field χ during inflation. It is taken to be initially misaligned from its minimum (taken to be at $\chi = 0$) to $\chi_0 \gg H_{\rm inf}$, where $H_{\rm inf}$ denotes the inflationary Hubble constant. Such a misalignment is robust as the field remains stuck due to the inflationary Hubble friction if its mass $m_\chi < H_{\rm inf}$. A well-motivated example of such a light field is an axion-like particle (ALP), which is a generic prediction of many BSM theories (see [16, 17]). During inflation, the energy density in χ, $V(\chi_0) \sim m_\chi^2 \chi_0^2$ is subdominant to that of the inflaton ϕ, which primarily drives inflation. After inflation, when the dropping Hubble constant matches m_χ, the χ field starts oscillating around its minimum and reheats some extension of the standard model (SM), including dark matter (DM), at $t_{\chi\rm reh}$. We will assume that this extension of the SM undergoes a first-order phase

JHEP06(2023)029

transition (PT) in the multi-TeV range, capable of producing an observable GWB, as is known to take place in many explicit SM extensions (see [1, 2]). If the reheat temperature from χ decay is higher than the PT temperature, the decay products of χ will undergo this phase transition. We will therefore refer to this sector emerging from χ decay as the "PT sector".

The inflaton on the other hand is taken to reheat another sector that interacts very weakly with the PT sector and does not participate in the phase transition, henceforth referred to as the "non-PT sector". The non-PT sector is taken to decay to the SM + DM at $t_{\rm dec}$ sometime after the phase transition but before DM decoupling. In this way, after the decay there is a single SM+DM sector which dominantly originates from inflaton ϕ reheating, assuming that the PT sector is subdominant to the non-PT sector as depicted in figure 1. On the other hand, the GWB dominantly originates from χ reheating. Therefore it is possible for the fluctuations in GWB to be distinct from those in the SM+DM, as we detail below.

2.1 Fluctuations

Here, we relate the anisotropies in the CMB and GWB to the independent primordial fluctuations ζ_ϕ and ζ_χ,[2]

$$\zeta_\phi(k) = \frac{H_{\rm inf}\delta\phi(k)}{\dot{\phi}_0}, \quad \zeta_\chi(k) = \frac{2\delta\chi(k)}{3\chi_0}\,, \tag{2.1}$$

where $\delta\phi \sim \delta\chi \sim H_{\rm inf}$, and the expressions are evaluated at the horizon exit of the co-moving mode k. The fluctuations in GWB will be dominated by the PT sector (reheated by χ), $\delta_{\rm GW} \sim \delta_{\rm PT} \sim \zeta_\chi$. More precisely, the anisotropies can be written in terms of the gauge-invariant fluctuations as [12, 20]

$$\delta_{\rm GW} = 4\zeta_\chi\left(1 - \frac{4}{3}f_{\rm PT}\right) - \frac{16}{3}\zeta_\phi\,, \tag{2.2}$$

where

$$f_{\rm PT} \equiv \frac{\rho_{\rm PT}}{\rho_{\rm total}} \tag{2.3}$$

is the fraction of energy density in the PT sector compared to the total energy density. Note that $\zeta_\phi \sim 10^{-5}$ sets the minimum $\delta_{\rm GW}$. This comes from the Sachs-Wolfe (SW) effect, which is dominated by the fluctuations of the non-PT sector. A small $\zeta_\chi < 10^{-5}$ would be swamped by the SW contribution, leaving the GWB to be predominantly adiabatic. On the other hand, large isocurvature in GWB coming from $\zeta_\chi > 10^{-5}$, would clearly imply the existence of a new light quantum field during inflation. Hence, we will focus on the range $\zeta_\chi > 10^{-5}$.

The fluctuations in the SM plasma (and hence in the CMB and matter distribution) after $t_{\rm dec}$ are a weighted superposition of the fluctuations in the PT sector and those in the decay

[2] A more relevant quantity to measure isocurvature is $\mathcal{S}_\chi = \zeta_\chi - \zeta_\phi$. However, for $\zeta_\chi \gg \zeta_\phi$, which is of interest to us in this work, we can simply take $\mathcal{S}_\chi \approx \zeta_\chi$.

JHEP06(2023)029

products of the non-PT sector, $\delta_\gamma \sim \delta_{\rm nPT}(t_{\rm dec}) + f_{\rm PT}\delta_{\rm PT}$. In terms of primordial fluctuations,

$$\delta_\gamma \approx -\frac{4}{5}\zeta_\phi - \frac{4}{5} f_{\rm PT}\zeta_\chi. \tag{2.4}$$

As expected, the contribution of ζ_χ to CMB can be kept small by choosing sufficiently small $f_{\rm PT}$. From the CMB observations [21], $\delta_\gamma \simeq 3.6 \times 10^{-5}$, giving a constraint

$$f_{\rm PT}\,\zeta_\chi \leq 4.5 \times 10^{-5}\,. \tag{2.5}$$

Therefore, since we are interested in $\zeta_\chi \gg 10^{-5}$, the PT sector must be sufficiently subdominant, $f_{\rm PT} \ll 1$. This leads to the simplification of eq. (2.2),

$$\delta_{\rm GW} \approx 4\zeta_\chi. \tag{2.6}$$

Additionally, if ζ_χ contains qualitative features which are not observed in CMB, the constraint on $f_{\rm PT}\,\zeta_\chi$ will be even stronger, requiring yet smaller $f_{\rm PT}$.

2.2 Strength of GWB and its anisotropies

During a first-order phase transition, gravitational waves are dominantly produced through bubble dynamics. It has been noted that the GW production is suppressed when the PT sector constitutes a smaller fraction of the total energy density at the time of the phase transition, i.e. $f_{\rm PT} < 1$ [22, 23]. In terms of the fraction of energy density in gravitational waves compared to the critical energy density at the time of production ($t_{\rm PT}$), the suppression goes as

$$\Omega_{\rm GW}(t_{\rm PT}) \equiv \frac{\rho_{\rm GW}(t_{\rm PT})}{\rho_{\rm total}(t_{\rm PT})} \approx f_{\rm PT}^2 \overline{\Omega}_{\rm GW}(t_{\rm PT}), \tag{2.7}$$

where $\overline{\Omega}_{\rm GW}$ represents GWB for a single sector system with $f_{\rm PT} = 1$. Intuitively, the amplitude of the gravitational wave must be $\mathcal{O}(f_{\rm PT})$, so that it vanishes in the absence of the PT plasma. Since GW energy density goes as the square of this amplitude, we expect $f_{\rm PT}^2$ scaling of the r.h.s. of eq. (2.7). We elaborate on this scaling in appendix A.

To estimate the strength of the GWB, we specialize to the plausible and relatively tractable scenario in which the gravitational waves are produced dominantly from bubble wall collisions in the envelope approximation.[3] Using eq. (2.7) and taking the expression for $\overline{\Omega}_{\rm GW}$ from [1], the GWB spectrum today can be given as[4]

$$\Omega_{\rm GW}^{(0)} h^2 \approx 1.67 \times 10^{-5} \tilde{\beta}^{-2} f_{\rm PT}^2 \left(\frac{\kappa \alpha_{\rm PT}}{1+\alpha_{\rm PT}}\right)^2 \left(\frac{100}{g_*(t_{\rm PT})}\right)^{1/3} \left(\frac{0.11 v_w^3}{0.42 + v_w^2}\right) S_{\rm bub}(\omega), \tag{2.8}$$

[3] In the case of significant coupling between the PT plasma and bubble walls, the majority of latent heat can be transferred to the plasma making sound waves the dominant source of gravitational waves. However, it turns out that for the parameters that we choose as the benchmark, i.e. $\alpha_{\rm PT} \sim 1$ and $\tilde{\beta} \sim 10$, the sound wave contribution will be similar in strength to the estimate in eq. (2.10) even if all the latent heat is transferred to the kinetic energy of the plasma [24].

[4] ref. [25] has pointed out that the peak energy density of the gravitational wave background from a phase transition can be enhanced if the small scale inhomogeneities ($H(t_{\rm PT}) < k < \beta$) in the PT plasma are large, i.e. $(\delta T/T) \gtrsim \tilde{\beta}^{-1}$. Since we consider relatively low $\tilde{\beta} = 10$ in all of our benchmarks, this effect is subdominant even for the biggest $\zeta_\chi \sim 10^{-2}$ on small scales that we will consider later. It will be important while considering more generic values of $\tilde{\beta} \sim \mathcal{O}(100)$. Also, note that this effect modifies the frequency spectrum, but does not affect the angular power spectrum which is the main focus of our work.

JHEP06(2023)029

where the frequency dependence is

$$S_{\rm bub}(\omega) = \frac{3.8(\omega/\omega_{\rm peak})^{2.8}}{1+2.8(\omega/\omega_{\rm peak})^{3.8}}\,. \tag{2.9}$$

Here, $\alpha_{\rm PT}$ is the ratio of the latent heat released compared to the energy density of the PT plasma before the phase transition, and κ is the efficiency of the latent heat transfer to bubble walls. We will take $\alpha_{\rm PT} \approx 1$, such that the efficiency $\kappa \approx 1$, and the bubble wall velocity $v_w \approx 1$. The peak frequency today $\omega_{\rm peak}$ can be estimated by redshifting the typical frequency at the time of phase transition ω_*, given by $\omega_* \approx 0.23\, H(t_{\rm PT})\, \tilde{\beta}$. We choose $\tilde{\beta} = 10$ for all our benchmarks. g_* corresponds to the effective number of relativistic degrees of freedom, and we take $g_*(t_{\rm PT}) \sim 100$.[5] Note that the envelope approximation is relatively crude and specific phase transitions may exhibit significant deviations.[6] However, it suffices for our purpose here since our main focus will be the angular power spectrum.

With the choice of parameters described above, the expression in eq. (2.8) at the peak frequency is simplified to

$$\Omega^{(0)}_{\rm GW} h^2 \approx 3.2 \times 10^{-9} f_{\rm PT}^2\,. \tag{2.10}$$

Following eq. (2.6), the size of the fluctuations in the GWB, which is relevant for detection, is

$$\delta\Omega^{(0)}_{\rm GW} h^2 \approx \Omega^{(0)}_{\rm GW} h^2 \times 4\zeta_\chi \approx 1.3 \times 10^{-8} f_{\rm PT}^2 \zeta_\chi\,. \tag{2.11}$$

The constraint of eq. (2.5) gives us an upper bound on the inhomogeneities of the GWB,

$$\delta\Omega^{(0)}_{\rm GW} h^2 \leq 5.8 \times 10^{-13} f_{\rm PT}\,. \tag{2.12}$$

Note that despite relative anisotropy $\delta\rho_{\rm GW}/\rho_{\rm GW} \sim \zeta_\chi$ being large $> 10^{-5}$, the absolute signal strength of the fluctuations is suppressed by one power of $f_{\rm PT}$, making it more difficult to detect.

3 Isocurvature GWB with an era of early matter dominance (eMD)

Smaller $f_{\rm PT}$ at $t_{\rm dec}$ allows for larger ζ_χ while evading constraints from CMB summarized in eq. (2.5). If both PT and non-PT sectors are radiation-dominated throughout, then this also constrains the PT sector to be subdominant by the same factor $f_{\rm PT}$ at the time of the phase transition, heavily suppressing the strength of GW produced, as seen in eqs. (2.10) and (2.12). This, however, will not be the case if there is a deviation from standard radiation dominance, for example, a period of early matter domination (eMD). In such modified cosmological histories, $f_{\rm PT}$ is effectively a function of time, and can be such that the PT sector is dominant during the phase transition and only becomes subdominant by $t_{\rm dec}$. We will show that this significantly enhances the strength of GWB compared to the purely-radiation-dominance scenario of [4], while still being consistent with constraints from CMB. For clarity, we define this time-dependent fraction as $\hat{f}(t)$, and its late time value at $t_{\rm dec}$ will continue to be denoted by $f_{\rm PT}$.

[5] In reality, $g_*(t_{\rm PT}) > 100$ depending on the exact extension of the SM undergoing the phase transition. However, this is a small effect considering the $g_*^{-1/3}$ dependence in eq. (2.8).

[6] See for example [26] for an updated numerical study of the phase transition in an abelian gauge theory with a comparison to the envelope approximation.

JHEP06(2023)029

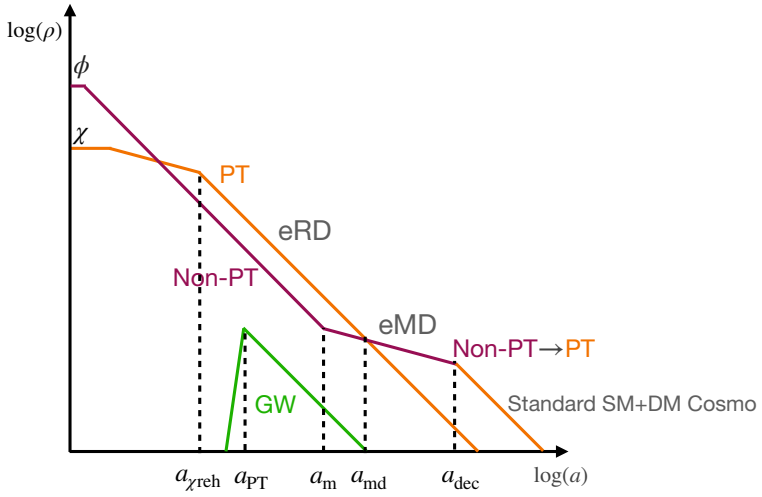

Figure 2. A schematic of the modified eMD model discussed in section 3 showing energy densities in various sectors as a function of the scale factor (time). While the decay products of the ALP χ are always radiation dominated, the massive particles (reheaton) in the decay products of the inflaton lead to a period of early matter domination.

Here we describe such a modified cosmological history with eMD, shown schematically in figure 2. As in the minimal model, the inflaton reheats the non-PT sector at the end of inflation, which dilutes like radiation, $\rho_{\mathrm{nPT}} \propto a^{-4}$. On the other hand, ρ_χ acts like matter while oscillating around its minimum, which dilutes slower than radiation. If the oscillations persist for a sufficiently long time, ρ_χ can dominate the energy density (as well as the curvature perturbations) of the universe before decaying to the PT sector, which subsequently undergoes the phase transition. Notice that unlike the radiation-dominated model described previously, the PT sector dominates the energy density during the phase transition, and therefore ρ_{GW} is not suppressed at production by f_{PT}. We will call this period of ρ_{PT} domination the era of early radiation domination (eRD).

Now we take the non-PT sector to be dominated by massive particles which become non-relativistic around t_{m}, sometime after the phase transition, redshifting slower than the radiation in the PT sector. The eRD of the PT sector is thereby replaced by eMD in the non-PT sector at t_{md}. The period of eMD ends at t_{dec} when the non-PT massive particles decay, reheating the SM+DM. We will therefore refer to these massive non-PT particles as "reheatons". The reheaton decays are taken to occur before DM decoupling, which allows thermalization with the SM and the remnants of the phase transition in the PT sector, matching onto the standard cosmological history from then on. In this way, we arrive at the following time-dependence of $\hat{f}_{\mathrm{PT}}$ from the $1/a^3$ redshifting of non-relativistic matter and the $1/a^4$ redshifting of relativistic radiation:

$$\hat{f}_{\mathrm{PT}}(t) = \begin{cases} (1+\epsilon)^{-1} & t_{\chi\mathrm{reh}} \le t \le t_m \\ \left(1+\epsilon\frac{a}{a_m}\right)^{-1} = \left(1+\frac{a}{a_{\mathrm{md}}}\right)^{-1} & t_m < t \le t_{\mathrm{dec}}\,, \end{cases} \tag{3.1}$$

where $\epsilon \equiv \left(\frac{\rho_{\mathrm{nPT}}}{\rho_{\mathrm{PT}}}\right)\Big|_{t_{\chi\mathrm{reh}}}$ and we have used $\epsilon(a_{\mathrm{md}}/a_m) = 1$. Therefore, $f_{\mathrm{PT}} \equiv \hat{f}_{\mathrm{PT}}(t_{\mathrm{dec}}) = (1 + a_{\mathrm{dec}}/a_{\mathrm{md}})^{-1} \approx (a_{\mathrm{md}}/a_{\mathrm{dec}})$.

JHEP06(2023)029

3.1 Strength of GW and anisotropies

In this model with eMD, the PT sector dominates the energy density at the phase transition, $\rho_{\rm total}(t_{\rm PT}) \approx \rho_{\rm PT}(t_{\rm PT})$ and $\hat{f}_{\rm PT}(t_{\rm PT}) \approx 1$. Hence, in eq. (2.8) for GW production at the time of the transition, $f_{\rm PT}^2$ is not a suppression.

However, the period of eMD dilutes GW radiation because of the differential redshifting of matter and GW radiation, such that

$$\frac{\rho_{\rm GW}(t_{\rm dec})}{\rho_{\rm total}(t_{\rm dec})} = \hat{f}_{\rm PT}(t_{\rm dec}) \frac{\rho_{\rm GW}(t_{\rm PT})}{\rho_{\rm total}(t_{\rm PT})} \,. \tag{3.2}$$

This, along with the same microphysical parameters as in section 2.2 for the phase transition, gives the fractional energy density in GWB today as

$$\Omega_{\rm GW}^{(0)} h^2 \approx 3.2 \times 10^{-9} f_{\rm PT} \,. \tag{3.3}$$

Note that the GW signal in this model, despite the dilution from eMD, has only one power of $f_{\rm PT}$ suppression, compared to the quadratic suppression in eq. (2.7).

The anisotropy of the GWB can again be related to the fluctuations of χ,

$$\delta_{\rm GW} \approx -\frac{4}{3}\zeta_\chi \,. \tag{3.4}$$

The factor in front of ζ_χ is smaller compared to eq. (2.6) because the SW contribution, in this case, comes from the PT sector itself, and is therefore anti-correlated with the inherent inhomogeneities of the GWB. The expression for the anisotropies of the CMB for all relevant scales (i.e., the scales that re-enter much after $t_{\rm dec}$) remains the same as eq. (2.4),

$$\delta_\gamma \approx -\frac{4}{5}\zeta_\phi - \frac{4}{5} f_{\rm PT} \zeta_\chi \,. \tag{3.5}$$

This is shown explicitly in section 4.1. The inhomogeneity in the GWB is then

$$\delta\Omega_{\rm GW}^{(0)} h^2 \approx \Omega_{\rm GW}^{(0)} h^2 \times \frac{4}{3}\zeta_\chi \approx 4.3 \times 10^{-9} f_{\rm PT} \zeta_\chi \,. \tag{3.6}$$

We must still satisfy the constraint in eq. (2.5). Saturating it gives

$$\delta\Omega_{\rm GW}^{(0)} h^2 \leq 1.9 \times 10^{-13} \,, \tag{3.7}$$

which is now independent of $f_{\rm PT}$, as opposed to eq. (2.12). The possibility that the relative anisotropies in the GWB are large while the absolute size of the anisotropic signal is unsuppressed by $f_{\rm PT}$, is the main result of our paper.

3.2 Peak frequency of GWB

The frequency spectrum of the GWB will be slightly shifted compared to the single-sector scenario ($f_{\rm PT} = 1$) due to the modified cosmological history. At production, the typical frequency of GWB for the choice of parameters given in section 2.2 is [1]

$$\omega_* \approx 0.23 \tilde{\beta} H(t_{\rm PT}). \tag{3.8}$$

JHEP06(2023)029

Red-shifting this frequency gives the peak frequency of the spectrum today

$$\begin{aligned}\omega_{\rm peak} &= \omega_* \left(\frac{a_{\rm PT}}{a_0}\right) \\ &\approx 0.23\tilde{\beta} \left(\frac{a_{\rm PT}}{a_0}\right) \left(\frac{H(t_{\rm PT})}{H(t_{\rm md})}\right) \left(\frac{H(t_{\rm md})}{H(t_{\rm dec})}\right) \left(\frac{H(t_{\rm dec})}{H(t_{eq})}\right) \left(\frac{H(t_{eq})}{H(t_0)}\right) H(t_0). \end{aligned} \tag{3.9}$$

Using $H \propto a^{-3/2}$ during matter dominance, while $H \propto a^{-2}$ during radiation dominance,

$$\begin{aligned}\omega_{\rm peak} &\approx 0.23\tilde{\beta} \left(\frac{a_{\rm PT}}{a_0}\right) \left(\frac{a_{\rm md}}{a_{\rm PT}}\right)^2 \left(\frac{a_{\rm dec}}{a_{\rm md}}\right)^{3/2} \left(\frac{a_{eq}}{a_{\rm dec}}\right)^2 \left(\frac{a_0}{a_{eq}}\right)^{3/2} H(t_0) \\ &\approx 2.8 \times 10^{-17} \tilde{\beta} \left(\frac{a_{eq}}{a_{\rm PT}}\right) f_{\rm PT}^{1/2} \text{ Hz}, \end{aligned} \tag{3.10}$$

where we have used the fact that the redshift at matter-radiation equality in the standard cosmological history $z_{eq} \approx a_{eq}^{-1} \approx 3100$, $H(t_0) \approx 2.2 \times 10^{-18}$ Hz, and $a_{\rm md}/a_{\rm dec} \approx f_{\rm PT}$ from eq. (3.1). Now,

$$\frac{a_{eq}}{a_{\rm PT}} = \frac{T_{\rm PT}(t_{\rm PT})}{T_{\rm SM}(t_{eq}))} f_{\rm PT}^{-1/4} \left(\frac{g_*(t_{\rm md})}{g_*(t_{\rm dec})}\right)^{1/4}. \tag{3.11}$$

Then with $T_{\rm SM}(t_{eq}) \sim 1\,\text{eV}$, $g_*(t_{\rm md}) \sim g_*(t_{\rm dec}) \sim 100$, and setting $\tilde{\beta} = 10$, we get

$$\omega_{\rm peak} \approx 2.8 \times 10^{-4} f_{\rm PT}^{1/4} \left(\frac{T_{\rm PT}(t_{\rm PT})}{\text{TeV}}\right) \text{ Hz}. \tag{3.12}$$

The dependence on $f_{\rm PT}$ is very mild, less than an order of magnitude in the range of $f_{\rm PT}$ that we will be led to consider. For a single sector ($f_{\rm PT} = 1$), a phase transition occurring at $T_{\rm PT}(t_{\rm PT}) \sim 100\,\text{TeV}$ gives $\omega_{\rm peak} \sim 28$ mHZ, falling within the sensitivity of LISA [3], BBO [27], and DECIGO [28]. As we lower the fraction of the PT sector to the smallest $f_{\rm PT} \sim 4.5 \times 10^{-4}$ of interest to us (see the last benchmark in table 1), the peak frequency shifts to $\omega_{\rm peak} \sim 4$ mHZ, remaining within the sensitivity of the above-mentioned detectors. In this case, an eMD starting shortly after the phase transition when $T_{\rm PT}(t_{\rm md}) \sim 32\,\text{TeV}$ ensures $T_{\rm SM}(t_{\rm dec}) \sim 100\,\text{GeV}$ and $f_{\rm PT} \sim 4.5 \times 10^{-4}$.

4 Gravitational crosstalk

The PT and non-PT sectors can influence each other gravitationally even though they are otherwise only weakly coupled. We want to ensure that the CMB scales are unaffected despite large perturbations in the PT sector during eRD era. We also want to identify other constraints on our eMD model which may arise from the evolution of perturbations after horizon re-entry. We address these two concerns here.

4.1 Modes that are superhorizon prior to $t_{\rm dec}$

Our modified early cosmology reverts to standard cosmology at $t_{\rm dec}$, where we will take $T_{\rm SM}(t_{\rm dec}) \gtrsim 100\,\text{GeV}$. We want to ensure that the observed fluctuation modes of the

JHEP06(2023)029

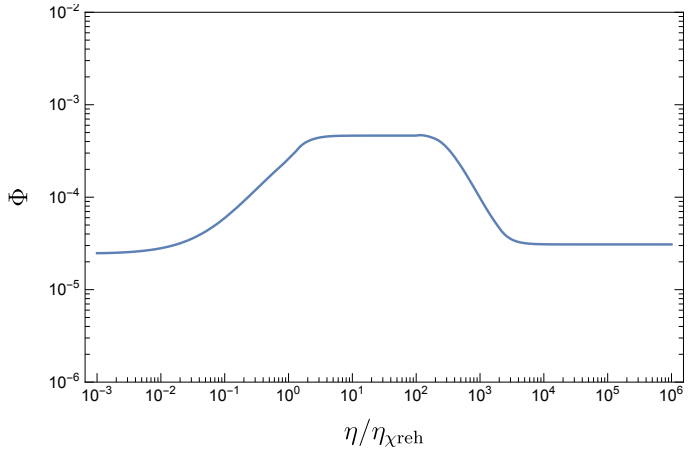

Figure 3. $\Phi(k)$ as a function of the conformal time η for a co-moving mode k that re-enters sufficiently after the end of eMD. We have taken a benchmark, $\zeta_\chi \approx 10^{-3}$, $f_{\rm PT} \approx 10^{-2}$, and $\epsilon = 1/2$. Conformal times denoting boundaries of different eras are $(\eta_{\rm m}/\eta_{\chi\rm reh}) \sim (\eta_{\rm md}/\eta_{\chi\rm reh}) \sim 100$ and $(\eta_{\rm dec}/\eta_{\chi\rm reh}) \sim 2000$.

CMB and LSS would be unaffected by the modified cosmology before $t_{\rm dec}$, and this is relatively straightforward to analyze because they are all superhorizon prior to $t_{\rm dec}$, given the high $T_{\rm SM}(t_{\rm dec})$.

We use the convention where the perturbed FLRW metric is given by [29],

$$g_{00} = -1 - 2\Psi, \quad g_{ij} = a^2(t)\delta_{ij}[1 + 2\Phi], \quad g_{0i} = 0\,. \tag{4.1}$$

In the absence of anisotropic stress, $\Phi = -\Psi$, and the relevant Einstein equation is

$$\eta\Phi' + \Phi + \frac{k^2\eta^2}{3}\Phi = \frac{1}{2}\sum_i f_i\delta_i\,, \tag{4.2}$$

where $'$ denotes partial derivative with respect to the conformal time η and k is the co-moving momentum. $f_i \equiv \rho_i/\rho_{\rm total}$ is the fraction of the energy density in the $i^{\rm th}$ sector and $\delta_i \equiv \delta\rho_i/\rho_i$ is the fractional density perturbation. When a certain mode is superhorizon, the k^2-term in eq. (4.2) can be neglected, giving

$$\eta\Phi' + \Phi = \frac{1}{2}\sum_i f_i\delta_i\,. \tag{4.3}$$

The gauge invariant fluctuation of a non-interacting fluid is conserved on superhorizon scales. For fluid i, it is given by

$$\zeta_i = \Phi + \frac{\delta_i}{3(1+w_i)}\,, \tag{4.4}$$

where w_i is its equation of state. Then $\zeta_{\rm nPT} = \zeta_\phi$ and $\zeta_{\rm PT} = \zeta_\chi$ remain constant until horizon re-entry. This also dictates the superhorizon evolution of radiation and matter density perturbations,

$$\delta'_{\rm rad} = -4\Phi', \quad \delta'_{\rm mat} = -3\Phi'\,. \tag{4.5}$$

JHEP06(2023)029

Using eqs. (4.3) and (4.5), we numerically evaluated the evolution of Φ for $\zeta_\chi \approx 10^{-3}$, $\zeta_\phi \approx 3.5 \times 10^{-5}$, and $f_{\rm PT} \approx 10^{-2}$, as shown in figure 3. While Φ is larger during eRD when the total curvature perturbation is dominated by ζ_χ, it becomes small again after eMD.[7] Let us do a few consistency checks. Eqs. (4.3) and (4.4) can be simplified to give $\Phi \approx \frac{2}{3}\zeta_{\rm total}$ during radiation dominance. Then we expect $\Phi \approx \frac{2}{3}\left(\frac{2}{3}\zeta_\chi + \frac{1}{3}\zeta_\phi\right) \approx 4.6 \times 10^{-4}$ (using $\epsilon = 1/2$) during eRD, while $\Phi \approx \frac{2}{3}\left(f_{\rm PT}\zeta_\chi + \zeta_\phi\right) \approx 3 \times 10^{-5}$ during radiation dominance after eMD. This is exactly what we find in figure 3. Therefore, the anisotropy in CMB (and in other late-time maps of adiabatic perturbations) remains small at 10^{-5} even in our modified scenario with PT sector domination during eRD.

4.2 Modes that have re-entered the horizon prior to $t_{\rm dec}$

In this section, we focus on the evolution of density perturbations in the non-PT sector and Φ for the modes that re-enter the horizon during eRD and eMD. This will be relevant for the constraints on ζ_χ on small scales, which can indirectly affect CMB or LSS.

The gradient terms that we neglected for superhorizon evolution become important as the mode becomes subhorizon. The coupled evolution of perturbations is given by

$$\begin{aligned} \eta\Phi' + \Phi + \frac{k^2\eta^2}{3}\Phi &= \frac{1}{2}\sum_i f_i\delta_i \\ \delta''_{\rm rad} + \frac{k^3}{3}\delta_{\rm rad} &= -4\Phi'' + \frac{4k^2}{3}\Phi \\ \delta''_{\rm mat} + \frac{1}{\eta}\delta'_{\rm mat} &= -3\Phi'' + k^2\Phi - \frac{3}{\eta}\Phi' \,. \end{aligned} \tag{4.6}$$

Let us start by analyzing the evolution of a co-moving mode that re-enters the horizon during eRD, generically labeled $k_{\rm eRD}$. Just before its re-entry, $\Phi(k_{\rm eRD}\eta \lesssim 1) \approx (2/3)\zeta_\chi$ as the PT sector is dominant. Since $\zeta_\phi = \Phi + \delta_{\rm nPT}/4 \sim 10^{-5}$ is conserved on superhorizon scales, we get $\delta_{\rm nPT}(k_{\rm eRD}\eta \lesssim 1) \approx -4(\Phi - \zeta_{\rm nPT}) \approx -(8/3)\zeta_\chi$ for $\zeta_\chi \gg \zeta_\phi$.

After the horizon re-entry at $\eta_{\rm eRD} \sim 1/k_{\rm eRD}$, perturbations follow eqs. (4.6). Below, we describe their qualitative behavior. Fluctuations in the radiation of the PT sector, $\delta_{\rm PT}$, oscillate in time with a constant amplitude throughout eRD and eMD. The behaviour of Φ and $\delta_{\rm nPT}$, however, changes significantly. During eRD, $|\Phi| \propto \eta^{-2}$ drops rapidly, while the amplitude of $\delta_{\rm nPT}$ remains constant when the non-PT sector is radiation-dominated and increases logarithmically $\sim \log(a)$ when it becomes matter-dominated. This logarithmic growth is insignificant if ϵ is close to 1, which we take to be the case. The linear growth during eMD, however, is significant when $\delta_{\rm nPT} \propto a$, and consequently Φ becomes constant. In summary,

$$|\delta_{\rm nPT}(k_{\rm eRD})| \approx \begin{cases} \dfrac{8}{3}\zeta_\chi & \eta_{\rm eRD} \le \eta < \eta_{\rm md} \\ 2\dfrac{\eta^2}{\eta_{\rm md}^2}\zeta_\chi & \eta_{\rm md} \le \eta < \eta_{\rm dec} \\ \dfrac{8}{3}\dfrac{\eta_{\rm dec}^2}{\eta_{\rm md}^2}\zeta_\chi & \eta_{\rm dec} \le \eta \,, \end{cases} \tag{4.7}$$

[7] A similar conclusion was found in [30]. They consider a model with two curvatons where one of the curvatons with larger perturbations dominates the energy density during an earlier era of radiation domination.

JHEP06(2023)029

where we have used the adiabatic relation $\delta_{\rm rad}/4 = \delta_{\rm mat}/3$ at the transitions between radiation and matter dominance, and $a \propto \eta^2$ during MD. Similarly, the behaviour of Φ can be given as

$$|\Phi(k_{\rm eRD})| \approx \begin{cases} \frac{2}{3}\frac{\eta_{\rm eRD}^2}{\eta^2}\zeta_\chi & \eta_{\rm eRD} \le \eta < \eta_{\rm md} \\ \frac{3}{5}\frac{\eta_{\rm eRD}^2}{\eta_{\rm md}^2}\zeta_\chi & \eta_{\rm md} \le \eta < \eta_{\rm dec} \\ \frac{2}{3}\frac{\eta_{\rm eRD}^2\eta_{\rm dec}^2}{\eta_{\rm md}^2\eta^2}\zeta_\chi & \eta_{\rm dec} \le \eta\,, \end{cases} \tag{4.8}$$

where we have used the fact that Φ decreases by a factor of (9/10) during a transition from RD to MD, and increases by (10/9) during a transition from MD to RD.

Now let us similarly analyze the evolution of perturbations for a co-moving mode $k_{\rm eMD}$ that re-enters during eMD. As $\hat{f}_{\rm PT}$ drops during eMD, the total density perturbation decreases, leading to a decreasing $\Phi(k_{\rm eMD})$ even on superhorizon scales. This can also be seen in figure 3. Using superhorizon conservation of $\zeta_{\rm nPT} = \zeta_\phi$, we see that the density perturbation $\delta_{\rm nPT} \sim -\Phi$ also decreases. After horizon re-entry, however, $\delta_{\rm nPT} \propto a$ increases while Φ remains constant till the end of the eMD era. Then

$$|\delta_{\rm nPT}(k_{\rm eMD})| \approx \begin{cases} 2\frac{(\eta_{\rm md}\eta)^2}{\eta_{\rm eMD}^4}\zeta_\chi & \eta_{\rm eMD} \le \eta < \eta_{\rm dec} \\ \frac{8}{3}\frac{(\eta_{\rm md}\eta_{\rm dec})^2}{\eta_{\rm eMD}^4}\zeta_\chi & \eta_{\rm dec} \le \eta\,, \end{cases} \tag{4.9}$$

and the evolution of Φ is

$$|\Phi(k_{\rm eMD})| \approx \begin{cases} \frac{4\hat{f}_{\rm PT}}{5+\hat{f}_{\rm PT}}\zeta_\chi + \frac{3(1-\hat{f}_{\rm PT})}{5+\hat{f}_{\rm PT}}\zeta_\phi \approx \frac{4\eta_{\rm md}^2}{5\eta_{\rm eMD}^2}\zeta_\chi + \frac{3}{5}\zeta_\phi & \eta_{\rm eMD} \le \eta < \eta_{\rm dec} \\ \frac{\eta_{\rm dec}^2}{\eta^2}\left[\frac{4f_{\rm PT}}{5}\zeta_\chi + \frac{4}{5}\zeta_\phi\right] \approx \frac{\eta_{\rm dec}^2}{\eta^2}\left(\frac{4}{5}\frac{\eta_{\rm md}^2}{\eta_{\rm eMD}^2}\zeta_\chi + \frac{4}{5}\zeta_\phi\right) & \eta_{\rm dec} \le \eta\,. \end{cases} \tag{4.10}$$

Here, we have used $f_{\rm PT} \ll 1$. The results of this section will be useful while analyzing constraints on our eMD model, which we discuss next.

4.2.1 Structure on small scales

The density perturbations in the non-PT sector grow during eMD as seen in eqs. (4.7) and (4.9). These overdensities will be retained and transferred to the SM+DM plasma after the reheaton decay. This poses the danger of overabundance of small-scale structures like compact mini-halos in the late universe. In reality, however, various processes at play during the decay of reheaton and DM decoupling suppress these small-scale fluctuations, effectively erasing any accumulated growth from the eMD era. We list the relevant processes below:

1. Refs. [31, 32] showed that the perturbative decay of the reheaton into radiation suppresses the amplitude of radiation perturbations by as much as $\sim 10^{-3}$ for subhorizon modes $k \gtrsim 20 k_{\rm dec}$.

JHEP06(2023)029

2. Frictional damping and acoustic oscillations during kinetic decoupling, and the free-streaming of DM afterwards erases DM fluctuations on all length scales smaller than the maximum of the horizon size at decoupling and the free-streaming length-scale [33, 34]. These effects erase enhancement in DM perturbations for all modes $k \gtrsim k_{\rm dec}$ that re-entered during eRD and eMD.

3. Finally, large perturbations in the baryon and photon plasma are erased by Silk damping [35, 36], and thus do not contribute to additional small-scale structure.

These mechanisms that erase DM perturbations on small scales require DM to be in thermal equilibrium with the SM at the time of reheaton decay. Our choice of $T_{\rm SM}(t_{\rm dec}) \gtrsim 100\,{\rm GeV}$ ensures that a standard WIMP-like DM candidate would satisfy this criterion. In summary, enhanced structure formation on small scales can be easily avoided in our eMD model by taking appropriately high reheat temperature for the SM at $t_{\rm dec}$.

4.2.2 Primordial black holes

Horizon patches with sufficient overdensity can collapse to form primordial black holes (PBH) in the early universe, which cannot be erased by the mechanisms discussed above. PBH production from adiabatic perturbations $\sim 10^{-5}$ is negligible. However, in our modified model, larger density perturbations during eRD and eMD era will enhance PBH production, giving a constraint on the power spectrum of χ on small scales.

During radiation dominance, the Hubble patches exceeding a certain critical overdensity (δ_c) collapse to form PBH. At a given time, the fraction of such collapsing patches can then be given as [37]

$$\beta_{\rm rad} = \int_{\delta_c}^{\infty} P(\delta) d\delta \approx \frac{\sigma}{\delta_c} \exp\left(-\frac{\delta_c^2}{2\sigma^2(M_H)}\right) . \tag{4.11}$$

Here M_H is the horizon mass and $\sigma^2(M_H)$ is the variance of the mass overdensities of Hubble patches, which is related to the power spectrum of the curvature perturbations $\mathcal{P}_{\mathcal{R}}$,[8]

$$\sigma^2(M_H) \equiv \langle (\delta M/M_H)^2 \rangle = \frac{16}{81} \int_0^{\infty} (q/k)^2 j_1^2(q/(\sqrt{3}k)) \tilde{W}^2(q/k) \mathcal{P}_{\mathcal{R}} \frac{dq}{q} . \tag{4.12}$$

Here, j_1 is the spherical Bessel function, and $\tilde{W}(q/k)$ is the Fourier transform of a window function used to smooth density contrast over the length scale $k^{-1} \sim (aH)^{-1}$. During eRD, $\mathcal{P}_{\mathcal{R}} \approx \mathcal{P}_{\chi}$. A real-space top hat window function in eq. (4.12) gives $\sigma^2(M_H) \sim 1.1\mathcal{P}_{\chi}$ [38]. The value of δ_c can vary between $0.4 - 0.7$ depending on the density distribution within the collapsing patch [39], but we take $\delta_c \approx 0.4$ for a conservative estimate. PBH formation during radiation era is thought to follow the phenomenon of critical collapse, which produces a distribution of PBH up to arbitrary low masses [37, 40–42],

$$M_{\rm PBH} = M_H(\delta - \delta_c)^{\gamma} . \tag{4.13}$$

[8] The power spectrum for any gauge-invariant perturbation 'i' is defined as

$$\langle\, \zeta_i(\vec{k}) \zeta_i(\vec{k}')\, \rangle \equiv \delta(\vec{k} + \vec{k}') \frac{(2\pi)^3}{k^3} \mathcal{P}_i(k) ,$$

For a scale-invariant spectrum, $\mathcal{P}(k)$ is constant.

JHEP06(2023)029

The most stringent constraint in the low mass region comes from CMB distortions caused by the evaporation of light PBH. This puts a constraint on their formation probability $\beta_{\rm eRD} \lesssim 10^{-25}$ [43, 44]. From eqs. (4.11) and (4.12), this translates to a bound $\zeta_\chi \lesssim 0.04$ on small scales (high k). A more significant enhancement of PBH formation occurs during the eMD era. This gives a stronger bound on small-scale ζ_χ, which we discuss below.

Density perturbations in the non-PT sector would grow linearly during MD, $\delta_{\rm nPT} \propto a(t)$, as discussed in section 4.2. Thus, even small perturbations can lead to significant PBH formation. When the perturbation becomes non-linear $\delta_{\rm nPT} \gtrsim \mathcal{O}(1)$, the corresponding Hubble patch separates from the background expansion and eventually collapses. A conservative bound on small-scale ζ_χ can then be obtained by simply requiring that the perturbations never become nonlinear during eMD, i.e.,

$$\delta_{\rm PT}\left(\frac{a_{\rm dec}}{a_{\rm md}}\right) \approx 4\zeta_\chi f_{\rm PT}^{-1} < 1. \tag{4.14}$$

Taking $\zeta_\chi f_{\rm PT} \lesssim 4\times10^{-5}$ from eq. (2.5), we get an upper bound on *small-scale* $\zeta_\chi < 3\times10^{-3}$. Note that this upper bound becomes tighter if the eMD lasts longer. However, this simple bound is too restrictive and a more careful analysis gives a fairly $f_{\rm PT}$-independent bound $\zeta_\chi < 10^{-2}$ on small scales. We elaborate on this below.

It was shown in [45, 46] that despite over-densities becoming nonlinear, only patches with sufficient spherical symmetry and homogeneity can collapse to form PBH.[9] The probability of PBH formation on the co-moving scale k^{-1} is then

$$\beta_{\rm mat}(k) \approx 0.2\left(\frac{r_{\rm sch}}{r_k}\right)^{13/2}, \tag{4.15}$$

where $r_k \sim a/k$ is the physical wavelength of the mode and $r_{\rm sch}$ is the Schwarzschild radius corresponding to the typical overdense region on length scale r_k. The ratio $(r_{\rm sch}/r_k) \approx \delta_{\rm nPT}(k,t)(aH/k)^2$ remains constant during eMD due to the linear growth of $\delta_{\rm nPT}$. Hence, the ratio can be evaluated at horizon re-entry for the modes re-entering during eMD, while for the modes that have re-entered before eMD, the ratio is evaluated at the start of eMD. From eqs. (4.7) and (4.9), we get

$$\frac{r_{\rm sch}}{r_k} \approx \begin{cases} \delta_{\rm nPT}(k,a_{\rm md})\left(\dfrac{a_k}{a_{\rm md}}\right)^2 \approx 2\zeta_\chi\left(\dfrac{a_k}{a_{\rm md}}\right)^2 & k \geq k_{\rm md} \\ \delta_{\rm nPT}(k,a_k) \approx 2\zeta_\chi\left(\dfrac{a_{\rm md}}{a_k}\right) & k_{\rm md} > k > k_{\rm dec}, \end{cases} \tag{4.16}$$

where a_k (t_k) corresponds to the scale factor (time) at the horizon re-entry of the co-moving mode k, and we have used $H \propto a^{-2}$ during RD while $H \propto a^{-3/2}$ during MD. Clearly, the largest β corresponds to the mode re-entering at the start of eMD, $k_{\rm md}$, with $\beta_{\rm mat}(k_{\rm md}) \approx 18\zeta_\chi^{13/2}$.

The mass of PBH formed from a certain comoving mode k during the matter domination era is roughly the horizon mass at reentry. Unlike radiation, pressureless matter does not

[9] The patches that do not satisfy these criteria form pancake/cigar-shaped structures instead. These are later dispersed due to the radiation pressure when the non-PT sector decays to SM.

JHEP06(2023)029

seem to follow critical collapse [47–49]. For the modes that re-enter during eRD but form PBH during eMD, the PBH mass is instead the mass within a patch of radius $\sim a_{\rm md}\, k^{-1}$ at the start of eMD. Thus

$$M_{\rm PBH}|_{\rm eMD} \approx \begin{cases} M_H(a_k)\left(\frac{a_k}{a_{\rm md}}\right) & k \geq k_{\rm md} \\ M_H(a_k) & k_{\rm md} > k > k_{\rm dec}. \end{cases} \tag{4.17}$$

Modes re-entering after eMD have curvature perturbation $\sim 10^{-5}$ as shown in section 4.1, and produce negligible amount of PBH following eq. (4.11). However, the modes that re-entered earlier during eRD and eMD retain larger perturbations even in the standard radiation-dominated era (sRD) after eMD, until they are erased by mechanisms discussed in section 4.2.1. We will show that despite large perturbations, there is no additional enhancement in PBH formation from these modes in the sRD. The collapse probability of a subhorizon mode in sRD can be estimated by performing Jeans mass analysis. Balancing kinetic and gravitational potential energy gives the Jeans mass $M_J = 2r/G$ for a spherical region of radius r. (Here, G is the gravitational constant.) The condition for instability $M > M_J$ then gives the critical overdensity for subhorizon modes,

$$\delta_c = \frac{1}{2G\rho r^2} = \frac{1}{2\pi^2 G\rho}\frac{k^2}{a^2}\,, \tag{4.18}$$

where we have taken $r = \pi a/k$. Using $8\pi G\rho = 3H^2$, the critical overdensity at some time t during sRD is

$$\delta_c = \frac{4}{3\pi}\left(\frac{k^2}{(aH)^2}\right) = \frac{4}{3\pi}\left(\frac{(a_k H_k)^2}{(aH)^2}\right) = 0.43\left(\frac{a_{\rm dec}}{a_k}\right)\left(\frac{a}{a_{\rm dec}}\right)^2. \tag{4.19}$$

Note that the critical overdensity is bigger for subhorizon modes than the constant ≈ 0.4 we had taken before. Now, $\delta_{\rm nPT}(k,t) = \delta_{\rm nPT}(k,t_k)(a_{\rm dec}/a_k)$ due to the linear growth during eMD. Thus the ratio

$$\frac{\delta_c(t)}{\delta_{\rm nPT}(k,t)} \approx \frac{0.43}{\delta_{\rm nPT}(k,t_k)}\left(\frac{a}{a_{\rm dec}}\right)^2 \geq \frac{0.43}{\delta_{\rm nPT}(k_{\rm md},t_{\rm md})} \tag{4.20}$$

is smallest at $t \approx t_{\rm dec}$ and for the co-moving mode $k_{\rm md}$. Using eqs. (4.11) and (4.12), the probability of collapse of the subhorizon modes during sRD is then

$$\beta_{\rm sRD} \lesssim \exp\left(-\frac{0.43^2}{2(1.1\mathcal{P}_\chi)}\right). \tag{4.21}$$

Following the analysis at the beginning of this section, we see that this production probability is much smaller than that from the eMD era.

Having analyzed PBH production, let us connect it to the experimental bounds on the fraction of PBH today,

$$f_{\rm PBH} \equiv \frac{\Omega^{(0)}_{\rm PBH}}{\Omega^{(0)}_{\rm DM}} = \int dM\psi(M). \tag{4.22}$$

JHEP06(2023)029

Here $\Omega_{\rm DM}^{(0)} \approx 0.26$ and the mass function $\psi(M)$ is defined as

$$\psi(M) = \frac{1}{\Omega_{\rm DM}^{(0)}} \frac{dn}{d\ln M} = \frac{1}{\Omega_{\rm DM}^{(0)} M} \beta(M) \left(\frac{a_{\rm eq}}{a_{\rm dec}}\right). \tag{4.23}$$

The factor of $(a_{\rm eq}/a_{\rm dec})$ in the above equation accounts for the relative enhancement of PBH abundance during the radiation dominated era since PBH dilute slower like pressureless matter. The mass of PBH can be evaluated using eq. (4.17) along with the relation $\rho_{\rm total} \approx 3H^2 M_{\rm pl}^2$, giving

$$M_{\rm PBH}(k) \sim \begin{cases} 10^{-6} M_\odot \left(\dfrac{a_k}{a_{\rm md}}\right)^3 f_{\rm PT}^{3/2} \left(\dfrac{100{\rm GeV}}{T_{\rm SM}(t_{\rm dec})}\right)^2 & k \geq k_{\rm md} \\ 10^{-6} M_\odot \left(\dfrac{a_k}{a_{\rm dec}}\right)^{3/2} \left(\dfrac{100{\rm GeV}}{T_{\rm SM}(t_{\rm dec})}\right)^2 & k_{\rm md} > k > k_{\rm dec}\,. \end{cases} \tag{4.24}$$

Here, $M_\odot$ corresponds to the solar mass and we have used $M_{\rm pl} \sim 10^{-39} M_\odot$.

Constraints on PBH are typically given for a monochromatic mass function, [43, 44]

$$\psi_{\rm mono} = f_{\rm PBH}\, \delta(M - M_c). \tag{4.25}$$

Figure 4 (b) shows these constraints as blue regions. The same constraints can also be used to check the viability of an extended mass function following the method of [50], which translates to the following condition

$$\int dM \frac{\psi(M)}{f_{\rm mono}(M)} \leq 1. \tag{4.26}$$

Here, $f_{\rm mono}$ is the maximum allowed fraction for a monochromatic mass function.

To evaluate the largest allowed ζ_χ on small scales, we have chosen two benchmarks saturating the limit in eq. (2.5) and assuming a scale-invariant spectrum:

1. $\zeta_\chi \approx 5 \times 10^{-3}$, $f_{\rm PT} \approx 9 \times 10^{-3}$, and $T_{\rm SM}(t_{\rm dec}) = 100\,{\rm GeV}$ (purple).
2. $\zeta_\chi \approx 10^{-2}$, $f_{\rm PT} \approx 4.5 \times 10^{-3}$, and $T_{\rm SM}(t_{\rm dec}) = 300\,{\rm GeV}$ (orange).

The mass function for these benchmarks is shown in figure 4 (a). We have checked that both of these benchmarks satisfy the criterion in eq. (4.26). It is clear that PBH production constraints $\zeta_\chi \lesssim 10^{-2}$ on small scales.

For a quick and more intuitive comparison with the constraints, we can take advantage of the roughly monochromatic appearance of our mass functions. In figure 4 (b), we therefore indicate where their monochromatic best fits would lie. While these points are so close to the constraints that the more refined criterion of eq. (4.26) is necessary to confidently check that our benchmarks are not excluded, what is clear is that the most relevant constraints are from microlensing.

Interestingly, our eMD model produces a sharply peaked PBH mass function without any sharp peaks in either $\mathcal{P}_{\zeta_\chi}$ or $\mathcal{P}_{\zeta_\phi}$. The peak corresponds to PBH produced from $k_{\rm md}$ (i.e. the co-moving mode that re-enters right at the start of eMD). Such a spectrum is typically achieved by introducing a scale-invariance-breaking feature in the inflationary potential

JHEP06(2023)029

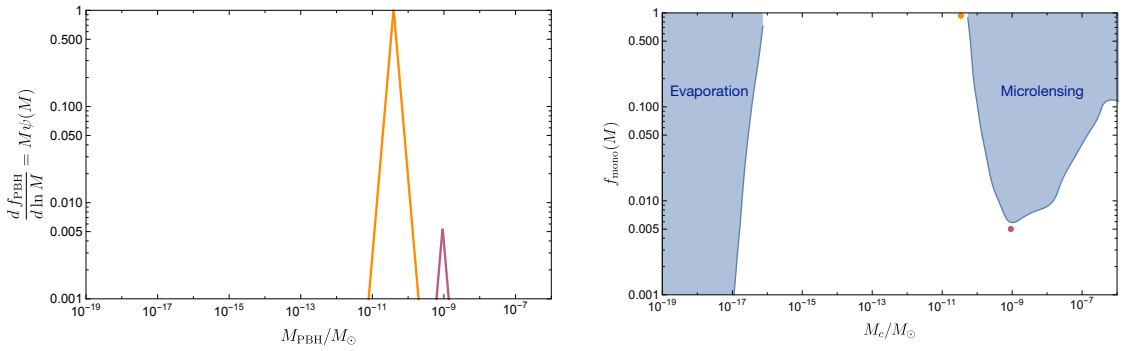

a) b)

Figure 4. (a) Fraction of DM energy density in PBH per logarithmic interval as a function of PBH mass in units of solar mass $M_\odot$. (b) Relevant constraints on monochromatic PBH mass functions from CMB distortions and microlensing (taken from [43, 44]). In (a), we show PBH mass distributions for two benchmarks in our eMD model: $\zeta_\chi \approx 5 \times 10^{-3}$, $f_{\rm PT} \approx 9 \times 10^{-3}$, $T_{\rm SM}(t_{\rm dec}) = 100\,{\rm GeV}$ in purple, and $\zeta_\chi \approx 10^{-2}$, $f_{\rm PT} \approx 4.5 \times 10^{-3}$, $T_{\rm SM}(t_{\rm dec}) = 300\,{\rm GeV}$ in orange. Noting the roughly monochromatic shape of these distributions, we have also shown their monochromatic best fits in (b) for an intuitive comparison with the constraints.

that can significantly enhance power at a specific k. In our model, the same can be achieved simply by the interplay of energy densities of two sectors, where both have scale-invariant fluctuations albeit of different amplitudes. Also note that for the second benchmark, PBH can make up the entirety of DM. A larger PBH fraction can be obtained at lower $T_{\rm SM}(t_{\rm dec})$ by taking smaller $f_{\rm PT}$ (and not saturating eq. (2.5)). Generally, $\zeta_\chi \lesssim 10^{-2}$ is required to avoid overproduction of PBH. The exact bound depends on the values of $T_{\rm SM}(t_{\rm dec})$ and $f_{\rm PT}$ as they can shift the location of the peak, exposing it to stricter constraints. However, eqs. (4.15) and (4.16) suggest that even moderately smaller ζ_χ will be sufficient to evade these constraints.

In conclusion, we require $\zeta_\chi \lesssim 10^{-2}$ on *small scales* to avoid overproduction of PBH. If the power spectrum of χ is nearly scale-invariant, as we have considered in this paper for simplicity, this also constrains ζ_χ and $\delta_{\rm GW}$ on the *large scales* relevant for GW detectors. However, $\zeta_\chi \gtrsim 10^{-2}$ on large scales can be made consistent with PBH constraints if the power spectrum is significantly red-tilted. This would require special model-building for χ potential, which we do not consider in this paper.

4.2.3 Scalar-induced gravitational waves

A weaker gravitational wave background can be induced by curvature perturbations at second order in perturbation theory (see [51] for a recent review). Larger curvature perturbations and the presence of eMD can enhance its production.[10] Here, we estimate the strength of such induced-GWB and compare it to the gravitational waves from the phase transition.

[10]Enhancement of primordial GWB in the presence of eMD generated by $f(R)$ gravity has been studied in [52].

JHEP06(2023)029

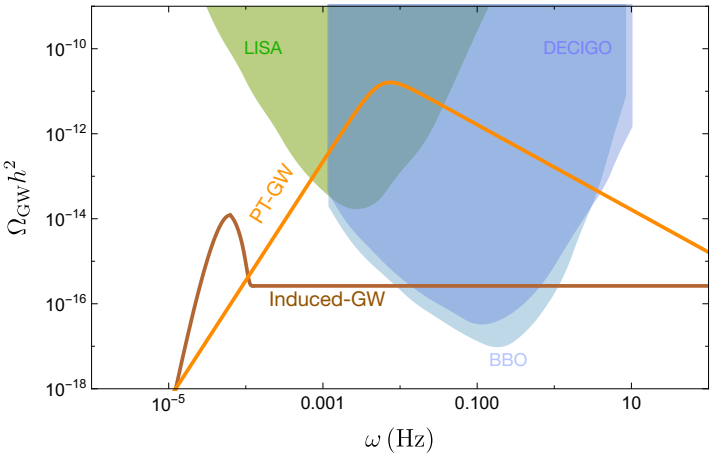

Figure 5. Strength of the GWB from phase transition (orange) occurring at $T_{\rm PT}(t_{\rm PT}) \sim 100\,\text{TeV}$ and that induced from curvature perturbations at second order (brown), compared with the power-law integrated sensitivities of LISA, BBO, and DECIGO (taken from [54]). The GWBs are computed for the benchmark that saturates PBH constraint (see discussion in section 4.2.2) with $\zeta_\chi = 10^{-2}$, $f_{\rm PT} = 4.5 \times 10^{-3}$, and $T_{\rm SM}(t_{\rm dec}) = 300\,\text{GeV}$.

The fraction of energy density in the induced-GWB per logarithmic k is

$$\Omega_{\rm GW}^{\rm ind}(\eta, k) = \frac{1}{24}\left(\frac{k}{a(\eta)H(\eta)}\right)^2 \overline{\mathcal{P}_h(\eta, k)} \tag{4.27}$$

where $\overline{\mathcal{P}_h(\eta, k)}$ is the time-averaged tensor power spectrum. It is related to the power spectrum of curvature perturbations as

$$\mathcal{P}_h(\eta, k) = 4\int_0^\infty dv \int_{|1-v|}^{|1+v|} du \left[\frac{4v^2 - (1+v^2-u^2)^2}{4vu}\right]^2 [I(v,u,x)]^2 \mathcal{P}_\mathcal{R}(kv)\mathcal{P}_\mathcal{R}(ku) \tag{4.28}$$

where $u = |\vec{k} - \vec{k'}|/k$, $v = k'/k$, and $x \equiv k\eta$. $I(v,u,x)$ contains information about the dynamics of scalar and tensor perturbations and is given in ref. [53]. The curvature perturbations can be related to (first-order) Φ as

$$\mathcal{P}_\mathcal{R} = \left(\frac{5+3w}{3+3w}\right)^2 \mathcal{P}_\Phi \tag{4.29}$$

Thus, the magnitude of $\mathcal{P}_h \propto \mathcal{P}_\Phi^2$.

During radiation dominance, $\Phi(\eta, k) \propto 1/\eta^2$ decays quickly inside the horizon. Thus, induced-GW are dominantly produced at horizon re-entry for modes that re-enter deep in the eRD era. This is not the case for modes re-entering during eMD, since Φ remains constant even after horizon re-entry during eMD. The result is a relative enhancement of induced-GW during eMD compared to the case of pure radiation dominance.

JHEP06(2023)029

Refs. [53, 55, 56] have analysed production of induced-GW in matter dominance era for a scale-invariant $\mathcal{P}_\Phi$ that remains constant on super-horizon scales.[11] We borrow results of [53] with appropriate rescaling as explained below. While $\Phi(k) \sim \zeta_\chi$ remains constant for a superhorizon mode during eRD, it decreases during eMD till horizon re-entry as the PT sector becomes subdominant (see figure 3). After horizon re-entry, $\Phi(k)$ becomes constant again till the end of eMD, and this value depends on the time of re-entry for each mode. The dominant effect of this evolution of Φ on the strength of induced-GW is the k-dependent rescaling of the results in [53] by a factor $\lambda(k)$. This rescaling factor $\lambda(k)$ can be obtained by noting that $\mathcal{P}_h \propto \mathcal{P}_\Phi^2$, and using eq. (4.10),

$$\lambda(k) \approx \left[\frac{3}{2}\left(\frac{4\hat{f}_{\rm PT}(t_k)}{5+\hat{f}_{\rm PT}(t_k)}\right)\right]^4 \tag{4.30}$$

Then the strength of the induced-GW is given as

$$\frac{\Omega_{\rm GW}^{\rm sec(0)}(k)}{\mathcal{P}_\chi^2 \Omega_{\rm rad}^{(0)}} \approx \begin{cases} 0.8 f_{\rm PT} & k > 2k_{\rm md} \\ 0.8 f_{\rm PT} + \left(\dfrac{\lambda(k)}{14000}\left(\dfrac{k}{k_{\rm dec}}\right)^2 (1-2\tilde{k}^{-1})^4 \right. & \\ \qquad \left. \times \left[105\tilde{k}^2 + 72\tilde{k} + 16 - 32\tilde{k}^{-1} - 16\tilde{k}^{-2}\right]\right) & 2k_{\rm md} \geq k > k_{\rm md} \\ \dfrac{\lambda(k)}{14000}\left(\dfrac{k}{k_{\rm dec}}\right)^2 \left[1792\tilde{k}^{-1} - 2520 + 768\tilde{k} - 105\tilde{k}^2\right] & k_{\rm md} \geq k > k_{\rm dec} \end{cases} \tag{4.31}$$

where $\tilde{k} \equiv k/k_{\rm md}$. The frequency of the GW today can be related to the co-moving mode k as

$$\omega = \frac{k}{2\pi} \sim 1.5 \times 10^{-15}\left(\frac{k}{1{\rm Mpc}^{-1}}\right) {\rm Hz} \tag{4.32}$$

Figure 5 shows $\Omega_{\rm GW}$ from phase transition (orange) and that induced from curvature perturbations (brown) as a function of frequency. We have taken the largest $\zeta_\chi \approx 10^{-2}$ allowed on small scales from PBH consideration (see benchmark 2 from section 4.2.2). We see that the GW signal from phase transition is much larger than induced-GW. Decreasing ζ_χ will quickly make induced-GW signal undetectably small given its sensitive dependence on the curvature perturbations seen in eq. (4.31). Interestingly, while a small $f_{\rm PT}$ suppresses GW signal from the phase transition, it enhances induced-GW. We will explore this aspect of induced-GWB in future work.

[11] It was pointed out in [57] and [58] that the strength of the induced GW from eMD sensitively depends on the exact model for the decay of the matter at the end of eMD. It was observed that a slow decay process suppresses the induced GW signal compared to eq. (4.31), while a quick decay enhances the signal. We suspect that a typical perturbative decay of the reheaton will fall under 'slow decay', suppressing induced GW signal. However, we have taken a conservative estimate following [53].

JHEP06(2023)029

	Benchmarks		Radiation-dominance		eMD	
	ζ_χ	$f_{\rm PT}$	$\Omega^{(0)}_{\rm GW}h^2$	$\delta\Omega^{(0)}_{\rm GW}h^2$	$\Omega^{(0)}_{\rm GW}h^2$	$\delta\Omega^{(0)}_{\rm GW}h^2$
1)	10^{-4}	4.5×10^{-1}	6.5×10^{-10}	2.6×10^{-13}	1.5×10^{-9}	1.9×10^{-13}
2)	10^{-3}	4.5×10^{-2}	6.5×10^{-12}	2.6×10^{-14}	1.5×10^{-10}	1.9×10^{-13}
3)	10^{-2}	4.5×10^{-3}	6.5×10^{-14}	2.6×10^{-15}	1.5×10^{-11}	1.9×10^{-13}
4)	10^{-1}	4.5×10^{-4}	6.5×10^{-16}	2.6×10^{-16}	1.5×10^{-12}	1.9×10^{-13}

Table 1. Benchmarks showing the strength of GWB and its inhomogeneities in the pure radiation-dominance model of [4] and our eMD model. We take them to saturate the CMB bound in eq. (2.5) (that is, $\zeta_\chi f_{\rm PT} = 4.5\times10^{-5}$). For a scale-invariant spectrum, they are consistent with the constraints from PBH production discussed in section 4.2.2, except for benchmark 4, which would require significantly red-tilted spectrum for χ to evade constraints on small scales (high-k).

5 Benchmarks and observability

The energy density in any GWB is bounded by two considerations. Firstly, it contributes to $N_{\rm eff}$ as a species of dark radiation, but the $N_{\rm eff}$ constraint is relatively mild:

$$\rho_{\rm GW} < 0.1\rho_\gamma. \tag{5.1}$$

Since we are interested in the possibility of $\delta_{\rm GW} \gg 10^{-5}$, it necessitates an isocurvature origin for the GWB. The stronger bounds on isocurvature from CMB give

$$\delta\rho_{\rm GW} < 0.1\delta\rho_\gamma. \tag{5.2}$$

This can be translated to

$$\delta\Omega^{(0)}_{\rm GW}h^2 < 10^{-5}\Omega^{(0)}_\gamma h^2 \sim 2.5\times10^{-10}, \tag{5.3}$$

where $\Omega^{(0)}_\gamma h^2 \approx 2.5\times10^{-5}$. We choose benchmarks that satisfy this constraint and also show that our modified eMD scenario brings $\delta\Omega^{(0)}_{\rm GW}$ of the signal closer to this upper bound over a large range of anisotropies.

In table. 1, we consider benchmarks that saturate eq. (2.5), i.e. $\zeta_\chi f_{\rm PT} = 4.5\times10^{-5}$. Corresponding GWB signals and their inhomogeneities are computed for the radiation-dominated model of [4] using eqs. (2.10) and (2.12). The same quantities are also computed for our eMD scenario using eqs. (3.3) and (3.7). We see that both the isotropic GWB signal and the absolute inhomogeneities are comparable or larger in the eMD model for $\zeta_\chi \gtrsim 10^{-4}$.

Note that benchmark 4 in table 1 above apparently violates PBH bounds discussed in section 4.2.2. However, that analysis assumed approximately scale-invariant ζ_χ up to high-k modes that are relevant for PBH production. This is indeed the case for the minimal model of a light χ with fixed mass during inflation that we have considered. It is however possible that with non-minimal couplings, ζ_χ has a suppressed power at high k so that the PBH bounds are evaded while still having large $\delta_{\rm GW}$ at observable small k modes.

If the power spectrum of χ contains features that are not seen in the CMB, $\zeta_\chi f_{\rm PT} < 4.5\times10^{-5}$ is required (see for example [13]). This means that for the same ζ_χ, the fraction

JHEP06(2023)029

$f_{\rm PT}$ must be even smaller. For example, consider a case where the PT sector only makes up about 1% of the final SM+DM density perturbations, i.e. $\zeta_\chi f_{\rm PT} \approx 4.5 \times 10^{-7}$. Consider $\zeta_\chi \sim 10^{-4}$ and $f_{\rm PT} \sim 4.5 \times 10^{-3}$. Then in the radiation-dominance scenario, we get $\Omega^{(0)}_{\rm GW} \sim 6.5 \times 10^{-14}$ and $\delta\Omega^{(0)}_{\rm GW} \sim 2.6 \times 10^{-17}$. In our eMD scenario, on the other hand, $\Omega^{(0)}_{\rm GW} \sim 1.5 \times 10^{-11}$ and $\delta\Omega^{(0)}_{\rm GW} \sim 1.9 \times 10^{-15}$. Comparing this to the first benchmark in table 1 makes the advantage of our eMD model even more apparent. Such scenarios with smaller $f_{\rm PT}$ would require longer periods of eMD, and possibly lower $T_{\rm SM}(t_{\rm dec})$ or higher PT temperature. A lower $T_{\rm SM}(t_{\rm dec})$ can be made compatible with our analysis by choosing an appropriate DM model that freezes out below this reheat temperature.

To access the improvement in the detection prospect of anisotropies with the eMD model, let us compare the angular power spectrum of GWB to the corresponding angular sensitivity of experiments. The anisotropies of PT-GWB can be conveniently expressed in the multipole basis analogous to the CMB,

$$\langle \delta\Omega^{(0)}_{\rm GW}(\hat{n}) \delta\Omega^{(0)}_{\rm GW}(\hat{n}') \rangle = \sum_\ell \frac{(2\ell+1)}{4\pi} C_\ell^{\rm GW} P_\ell(\cos\theta)\,, \tag{5.4}$$

where $\hat{n}\cdot\hat{n}' = \cos\theta$ and P_ℓ are the Legendre polynomials. The angular power spectrum $C_\ell^{\rm GW}$ can be related to the amplitude of GW fluctuations as,

$$C_\ell^{\rm GW} = \frac{2}{\pi}\int_0^\infty \frac{dk}{k} \mathcal{P}_{\delta\Omega_{\rm GW}}(k) j_\ell^2[k(\eta_{\rm PT} - \eta_{\rm today})], \tag{5.5}$$

where j_ℓ are spherical Bessel functions and $\mathcal{P}_{\delta\Omega_{\rm GW}}$ is given by

$$\langle \delta\Omega^{(0)}_{\rm GW}(\vec{k}) \delta\Omega^{(0)}_{\rm GW}(\vec{k}') \rangle = \delta(\vec{k}+\vec{k}') \frac{(2\pi)^3}{k^3} \mathcal{P}_{\delta\Omega_{\rm GW}}(k). \tag{5.6}$$

For a scale-invariant spectrum, $\mathcal{P}_{\delta\Omega_{\rm GW}}(k)$ is constant. In this case, the integral in eq. (5.5) can be simplified [29], giving

$$\ell(\ell+1) C_\ell^{\rm GW} \approx 14 \mathcal{P}_{\delta\Omega_{\rm GW}} \tag{5.7}$$

$C_\ell^{\rm GW}$ can be directly compared to the noise power spectrum N_ℓ of a given experiment, which sets the lower limit for detectable GWB power spectra as a function of multipole ℓ. Figure 6 (b) shows $\ell(\ell+1)N_\ell$ as a function of multipole ℓ for relevant detectors like LISA, BBO, and ultimate-DECIGO, which were computed in ref. [59], and are based on the code of ref. [60]. The design of these space-based detectors gives higher sensitivity to even multipoles, resulting in the zigzag curves in the plot.

Figure 6 shows the strength of GWB signals for benchmarks 1 (red), 3 (orange), and 4 (yellow) from table 1 in the radiation-dominated (dotted lines) and eMD model (solid lines). Figure 6 (a) compares the strength of the GWB monopoles with the projected power-law integrated sensitivities for LISA, BBO, and DECIGO [54]. We have incorporated the shift in peak frequency following discussion in section 3.2 and appendix A. Figure 6 (b), on the other hand, illustrates the strength of the anisotropic GWB power spectrum (computed using eq. (5.7)) in the radiation-dominated and eMD models, against projections of the noise

JHEP06(2023)029

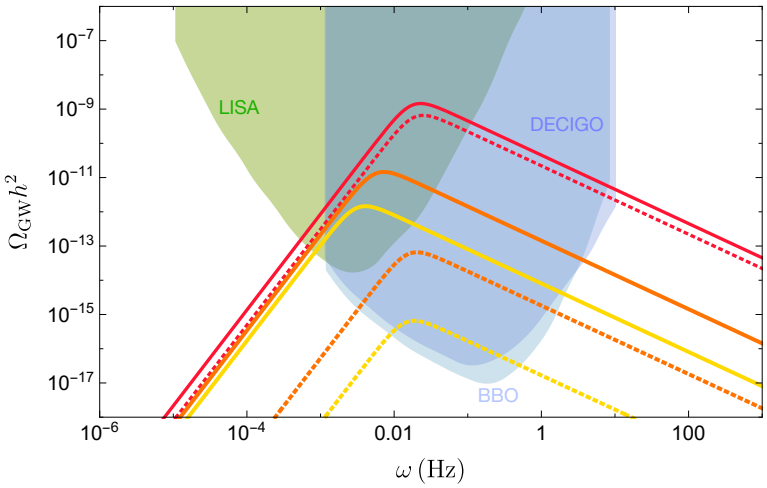

a) Isotropic part.

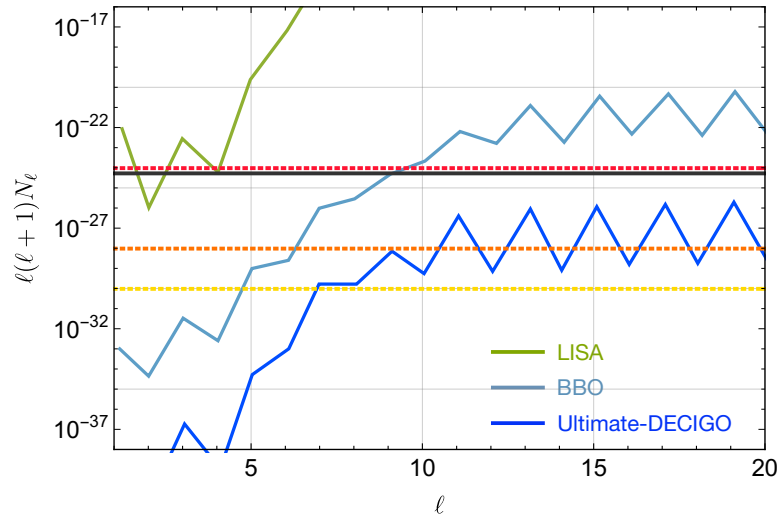

b) Anisotropies.

Figure 6. Comparison of benchmarks 1 (red), 3 (orange), and 4 (yellow) from table. 1 with the (a) sensitivities of upcoming space-based experiments like LISA, BBO, and DECIGO, and (b) noise power spectra N_ℓ as computed in [59]. Solid lines correspond to our modified eMD model while the dotted lines correspond the radiation-dominance scenario of [4]. In (a), the GWB spectra are evaluated for a phase transition occurring at $T_{\rm PT}(t_{\rm PT}) \sim 100\,\text{TeV}$ in a single-sector scenario, and contribution from bubble collisions is taken to be the dominant source of gravitational waves. In (b), all benchmarks for the eMD model lie on the same line at $\approx 5 \times 10^{-25}$ and are together represented by a black line.

JHEP06(2023)029

power spectrum for LISA, BBO, and ultimate-DECIGO configurations [59]. As explained before, there is no additional $f_{\rm PT}$ suppression in the GWB inhomogeneities in the eMD model, and the power spectrum for all the benchmarks lies at the same position $\approx 5 \times 10^{-25}$ shown as a black line in figure 6 (b).

6 Discussion

LISA is the most sensitive GW detector already under development, with a baseline sensitivity of $\Omega_{\rm LISA}h^2 \sim 10^{-12}$ [1, 3] and a power-law integrated sensitivity of $\Omega^{\rm int}_{\rm LISA}h^2 \sim 10^{-14}$ [54]. Clearly, it would be important to be able to see at least an isotropic GWB signal at LISA in order to motivate development of more futuristic proposed detectors, such as BBO or DECIGO, to measure the anisotropies. We see from figure 6 (a) that for larger fractional GWB anisotropies, even the isotropic component can be challenging at LISA for the radiation-domination models, whereas they can be readily detectable in our early-matter-domination (eMD) models.

Once an isotropic GWB is detected, there would be a *guaranteed* anisotropic component to be discovered. In fact we see in figure 6 (b) that with our eMD model, it is possible that the first few GWB multipoles might be visible already at LISA, above the instrumental noise anisotropy, for a much larger range of GWB anisotropies. Detection of a highly anisotropic GWB at LISA would make an even stronger case for more sensitive detectors to mine the physics of the isocurvature GWB map with higher multipoles. Figure. 6 (b) shows that such high resolution map-making would be possible within our eMD model. Finally, larger GWB signals in the eMD model will be significantly easier to distinguish from the various astrophysical foregrounds [61].

Acknowledgments

The authors would like to thank Peizhi Du, Anson Hook, Mrunal Korwar, Soubhik Kumar, Peter Shawhan, Gustavo Marques Tavares, and Lian-Tao Wang for useful discussions and comments. This work was supported by NSF grant PHY-2210361 and the Maryland Center for Fundamental Physics.

A $f_{\rm PT}^2$ suppression in $\Omega_{\rm GW}$ in the radiation-dominated model

A first-order phase transition proceeds through the formation and expansion of bubbles of true vacuum. The rate of bubble formation per unit volume Γ can be given by

$$\Gamma \sim T_{\rm PT}^4 e^{-S(T_{\rm PT})}, \tag{A.1}$$

where $T_{\rm PT}$ is the temperature of the PT sector and $S(T_{\rm PT})$ is the Euclidean action of a critical bubble. The transition begins when the rate of bubble formation is comparable to the Hubble rate, $\Gamma \sim H^4$. Now, in the radiation-dominated model described in section 2, the Hubble rate can be written in terms of $T_{\rm PT}$ as

$$H^2 \sim \frac{\rho_{\rm total}}{M_{\rm pl}^2} \sim \frac{f_{\rm PT}^{-1} T_{\rm PT}^4}{M_{\rm pl}^2}. \tag{A.2}$$

JHEP06(2023)029

Then the phase transition begins at temperature $T_* \equiv T_{\rm PT}(t_{\rm PT})$ such that

$$T_*^4 e^{-S(T_*)} \sim \frac{f_{\rm PT}^{-2} T_*^8}{M_{\rm pl}^4}$$
$$\implies \quad -S(T_*) \sim 4\log\left(\frac{T_*}{M_{\rm pl}}\right) - 2\log\left(f_{\rm PT}\right). \tag{A.3}$$

Since gravitational wave production in a single sector ($f_{\rm PT} = 1$) is well understood, we compare the multi-sector case of $f_{\rm PT} < 1$ with the single-sector case of $f_{\rm PT} = 1$. For this, we henceforth use '$\bar{}$' to denote quantities corresponding to a single-sector system. Then $-S(\overline{T}_*) \sim 4\log\left(\frac{\overline{T}_*}{M_{\rm pl}}\right)$. Now, let us expand $T_* = \overline{T}_* + \Delta T$. Then eq. (A.3) gives

$$-\left(\overline{\tilde{\beta}}\,\frac{\Delta T}{\overline{T}_*} + \left(\left.\frac{d\tilde{\beta}}{d\log T}\right|_{\overline{T}_*} - \overline{\tilde{\beta}}\right)\left(\frac{\Delta T}{\overline{T}_*}\right)^2\right) \sim 4\log\left(1 + \frac{\Delta T}{\overline{T}_*}\right) - 2\log f_{\rm PT}, \tag{A.4}$$

where,

$$\tilde{\beta} \equiv \left.\frac{\beta}{H}\right|_{t_{\rm PT}} = \left.\frac{dS}{d\log T}\right|_{T_*}. \tag{A.5}$$

$\tilde{\beta}$ is an important PT parameter as it determines the typical length/time scale of the bubble dynamics (and hence the typical frequency of gravitational waves at production) relative to H^{-1}. From eq. (A.4), we see that the temperature shift depends on $\overline{\tilde{\beta}}$. Therefore, let us consider two cases:

1) Typical $\overline{\tilde{\beta}} \sim \mathcal{O}(100)$: for a TeV scale phase transition, the typical value of $\overline{\tilde{\beta}} \sim S(\overline{T}_*) \sim \mathcal{O}(100)$. In this case, the change in the PT temperature is small and eq. (A.4) simplifies to

$$\frac{\Delta T}{\overline{T}_*} \approx \frac{2\log f_{\rm PT}}{\overline{\tilde{\beta}} + 4}. \tag{A.6}$$

For the smallest $f_{\rm PT} \sim 10^{-5}$ of interest, we get $(\Delta T/\overline{T}_*) \sim -0.1$. Now, the going rate for the change in $\tilde{\beta}$ is also expected to be set by the action, i.e. $(d\tilde{\beta}/d\log T)|_{\overline{T}_*} \sim S(\overline{T}_*) \sim \mathcal{O}(100)$. So the expected change in $\tilde{\beta}$ due to the shift in the PT temperature is $\Delta\tilde{\beta} \sim 10 \ll \overline{\tilde{\beta}}$. Thus, we can take

$$\tilde{\beta} \approx \overline{\tilde{\beta}}. \tag{A.7}$$

2) "Tuned" $\overline{\tilde{\beta}} \sim \mathcal{O}(10)$: from the observational perspective, gravitational waves from phase transitions with smaller $\tilde{\beta}$ are more likely to be observed first. Thus we have considered $\overline{\tilde{\beta}} = 10$ in this paper. This requires tuning of parameters such that the rate of change of the action is an order of magnitude smaller than the action itself at $\overline{T}_*$. Despite the tuning in $\overline{\tilde{\beta}}$, we still expect $(d\tilde{\beta}/d\log T)|_{\overline{T}_*} \sim \mathcal{O}(100)$. In other words, a shift in the PT temperature due to $f_{\rm PT} < 1$ is likely to take the system away from the tuned point to a more typical value of $\tilde{\beta} \sim \mathcal{O}(100)$. Taking $f_{\rm PT} \sim 10^{-5}$ in eq. (A.4) gives $(\Delta T/\overline{T}_*) \sim -0.4$ and $\Delta\tilde{\beta} \sim 40$. Now

JHEP06(2023)029

a larger $\tilde{\beta}$ will lead to an additional suppression in the GW signal on top of the expected $f_{\rm PT}^2$. This can be seen through the $\tilde{\beta}^{-2}$ dependence in eq. (2.8). However, since the exact shift in $\tilde{\beta}$ is model dependent, we make a conservative choice of neglecting change $\tilde{\beta}$ and follow eq. (A.7) even in the case of relatively small $\tilde{\beta}$. Note that correctly including the suppression due to larger $\tilde{\beta}$ will only strengthen the case for our eMD model described in section 3.

Let us now look at the gravitational wave emission, which is governed by the transverse traceless part of the linearized Einstein equations

$$\Box h_{\rm GW} \sim \frac{\mathcal{T}(x)}{M_{\rm pl}^2}\,, \tag{A.8}$$

where $\Box \equiv (\partial_t^2 + 3H\partial_t - a^{-2}\nabla^2)$ and $\mathcal{T}$ is the transverse traceless part of the stress-energy tensor of the PT sector. It is useful to change to dimensionless coordinates $\tilde{x} = Hx$ and the stress tensor $\tilde{\mathcal{T}} = \rho_{\rm PT}^{-1}\mathcal{T}$,[12] where $\tilde{\mathcal{T}}$ captures the dimensionless "shape" of the dominant quadrupole GW sources. Then

$$\tilde{\Box} h_{\rm GW} \sim \frac{\rho_{\rm PT}\tilde{\mathcal{T}}(\tilde{x})}{H^2 M_{\rm pl}^2} \sim f_{\rm PT}\tilde{\mathcal{T}}(\tilde{x})\,. \tag{A.9}$$

For the familiar case of $f_{\rm PT} = 1$, all the length/time scales of the dominant GW sources are set by β [1, 62, 63]. This means that the piece of $\tilde{\mathcal{T}}$ that is relevant for GW production is only parametrized by the dimensionless $\tilde{\beta}$. Given eq. (A.7), we then have

$$\tilde{\mathcal{T}}(\tilde{x}) \simeq \overline{\tilde{\mathcal{T}}}(\tilde{x})\,. \tag{A.10}$$

Thus, eq. (A.9) can be written as

$$\tilde{\Box} h_{\rm GW} \sim f_{\rm PT}\overline{\tilde{\mathcal{T}}}(\tilde{x})\,, \tag{A.11}$$

giving

$$h_{\rm GW}(\tilde{x}) \simeq f_{\rm PT}\overline{h}_{\rm GW}(\tilde{x}) \tag{A.12}$$

Now,

$$\begin{aligned}\Omega_{\rm GW} \equiv \frac{\rho_{\rm GW}}{\rho_{\rm total}} &\sim \frac{M_{\rm pl}^2(\partial h_{\rm GW})^2}{H^2 M_{\rm pl}^2} \\ &\sim (\tilde{\partial}\, h_{\rm GW})^2 \sim f_{\rm PT}^2\left(\tilde{\partial}\,\overline{h}_{\rm GW}\right)^2 \\ \implies \Omega_{\rm GW} &\approx f_{\rm PT}^2\overline{\Omega}_{\rm GW}\,,\end{aligned} \tag{A.13}$$

where we have used eq. (A.12) in the second line.

[12] Since we have taken $\alpha_{\rm PT} \approx 1$.

JHEP06(2023)029

The reader may wonder if the GW production from MHD turbulence shows different dependence on $f_{\rm PT}$ as the turbulence may cascade to smaller scales than β^{-1}. However, analytic calculations suggest that the dominant MHD contribution is still in frequencies $\sim \beta$ [62]. Thus, we expect the above analysis to hold also for MHD turbulence. The turbulence contribution is therefore expected to remain subdominant compared to the acoustic and bubble wall collision contributions even in the case $f_{\rm PT} < 1$.

JHEP06(2023)029

References

[1] C. Caprini et al., *Science with the space-based interferometer eLISA. II: Gravitational waves from cosmological phase transitions*, *JCAP* **2016** (2016) 001.

[2] A. Mazumdar and G. White, *Review of cosmic phase transitions: their significance and experimental signatures*, *Rept. Prog. Phys.* **82** (2019) 076901 [arXiv:1811.01948] [INSPIRE].

[3] LISA collaboration, *Laser Interferometer Space Antenna*, arXiv:1702.00786 [INSPIRE].

[4] M. Geller, A. Hook, R. Sundrum and Y. Tsai, *Primordial Anisotropies in the Gravitational Wave Background from Cosmological Phase Transitions*, *Phys. Rev. Lett.* **121** (2018) 201303 [arXiv:1803.10780] [INSPIRE].

[5] S. Olmez, V. Mandic and X. Siemens, *Anisotropies in the Gravitational-Wave Stochastic Background*, *JCAP* **07** (2012) 009 [arXiv:1106.5555] [INSPIRE].

[6] L. Bethke, D.G. Figueroa and A. Rajantie, *Anisotropies in the Gravitational Wave Background from Preheating*, *Phys. Rev. Lett.* **111** (2013) 011301 [arXiv:1304.2657] [INSPIRE].

[7] L. Bethke, D.G. Figueroa and A. Rajantie, *On the Anisotropy of the Gravitational Wave Background from Massless Preheating*, *JCAP* **06** (2014) 047 [arXiv:1309.1148] [INSPIRE].

[8] A.C. Jenkins and M. Sakellariadou, *Anisotropies in the stochastic gravitational-wave background: Formalism and the cosmic string case*, *Phys. Rev. D* **98** (2018) 063509 [arXiv:1802.06046] [INSPIRE].

[9] N. Bartolo et al., *Anisotropies and non-Gaussianity of the Cosmological Gravitational Wave Background*, *Phys. Rev. D* **100** (2019) 121501 [arXiv:1908.00527] [INSPIRE].

[10] N. Bartolo et al., *Characterizing the cosmological gravitational wave background: Anisotropies and non-Gaussianity*, *Phys. Rev. D* **102** (2020) 023527 [arXiv:1912.09433] [INSPIRE].

[11] L. Valbusa Dall'Armi et al., *Imprint of relativistic particles on the anisotropies of the stochastic gravitational-wave background*, *Phys. Rev. D* **103** (2021) 023522 [arXiv:2007.01215] [INSPIRE].

[12] S. Kumar, R. Sundrum and Y. Tsai, *Non-Gaussian stochastic gravitational waves from phase transitions*, *JHEP* **11** (2021) 107 [arXiv:2102.05665] [INSPIRE].

[13] A. Bodas and R. Sundrum, *Primordial clocks within stochastic gravitational wave anisotropies*, *JCAP* **10** (2022) 012 [arXiv:2205.04482] [INSPIRE].

[14] C.R. Contaldi, *Anisotropies of Gravitational Wave Backgrounds: A Line Of Sight Approach*, *Phys. Lett. B* **771** (2017) 9 [arXiv:1609.08168] [INSPIRE].

[15] R.K. Sachs and A.M. Wolfe, *Perturbations of a cosmological model and angular variations of the microwave background*, *Astrophys. J.* **147** (1967) 73 [INSPIRE].

[16] A. Ringwald, *Axions and Axion-Like Particles*, in the proceedings of the *49th Rencontres de Moriond on Electroweak Interactions and Unified Theories*, La Thuile Italy, March 15–22 (2014), p. 223–230 [arXiv:1407.0546] [INSPIRE].

[17] D.J.E. Marsh, *Axion Cosmology*, *Phys. Rept.* **643** (2016) 1 [arXiv:1510.07633] [INSPIRE].

[18] PLANCK collaboration, *Planck 2018 results. X. Constraints on inflation*, *Astron. Astrophys.* **641** (2020) A10 [arXiv:1807.06211] [INSPIRE].

[19] D. Baumann, *Inflation*, in the proceedings of the *Theoretical Advanced Study Institute in Elementary Particle Physics: Physics of the Large and the Small*, Boulder U.S.A., June 1–26 (2009), p. 523–686 [DOI:10.1142/9789814327183_0010] [arXiv:0907.5424] [INSPIRE].

[20] K.A. Malik and D. Wands, *Cosmological perturbations*, *Phys. Rept.* **475** (2009) 1 [arXiv:0809.4944] [INSPIRE].

[21] PLANCK collaboration, *Planck 2018 results. VI. Cosmological parameters*, *Astron. Astrophys.* **641** (2020) A6 [*Erratum ibid.* **652** (2021) C4] [arXiv:1807.06209] [INSPIRE].

[22] M. Breitbach et al., *Dark, Cold, and Noisy: Constraining Secluded Hidden Sectors with Gravitational Waves*, *JCAP* **07** (2019) 007 [arXiv:1811.11175] [INSPIRE].

[23] M. Fairbairn, E. Hardy and A. Wickens, *Hearing without seeing: gravitational waves from hot and cold hidden sectors*, *JHEP* **07** (2019) 044 [arXiv:1901.11038] [INSPIRE].

[24] M. Hindmarsh, S.J. Huber, K. Rummukainen and D.J. Weir, *Shape of the acoustic gravitational wave power spectrum from a first order phase transition*, *Phys. Rev. D* **96** (2017) 103520 [*Erratum ibid.* **101** (2020) 089902] [arXiv:1704.05871] [INSPIRE].

[25] R. Jinno, T. Konstandin, H. Rubira and J. van de Vis, *Effect of density fluctuations on gravitational wave production in first-order phase transitions*, *JCAP* **12** (2021) 019 [arXiv:2108.11947] [INSPIRE].

[26] M. Lewicki and V. Vaskonen, *Gravitational waves from colliding vacuum bubbles in gauge theories*, *Eur. Phys. J. C* **81** (2021) 437 [*Erratum ibid.* **81** (2021) 1077] [arXiv:2012.07826] [INSPIRE].

[27] G.M. Harry et al., *Laser interferometry for the big bang observer*, *Class. Quant. Grav.* **23** (2006) 4887 [*Erratum ibid.* **23** (2006) 7361] [INSPIRE].

[28] S. Kawamura et al., *The Japanese space gravitational wave antenna: DECIGO*, *Class. Quant. Grav.* **28** (2011) 094011 [INSPIRE].

[29] S. Dodelson and F. Schmidt, *Modern cosmology*, Academic Press (2020) [DOI:10.1016/C2017-0-01943-2].

[30] T. Suyama and J. Yokoyama, *Temporal enhancement of super-horizon curvature perturbations from decays of two curvatons and its cosmological consequences*, *Phys. Rev. D* **84** (2011) 083511 [arXiv:1106.5983] [INSPIRE].

[31] A.L. Erickcek and K. Sigurdson, *Reheating Effects in the Matter Power Spectrum and Implications for Substructure*, *Phys. Rev. D* **84** (2011) 083503 [arXiv:1106.0536] [INSPIRE].

JHEP06(2023)029

[32] J.J. Fan, O. Özsoy and S. Watson, *Nonthermal histories and implications for structure formation*, *Phys. Rev. D* **90** (2014) 043536 [arXiv:1405.7373] [INSPIRE].

[33] A. Loeb and M. Zaldarriaga, *The Small-scale power spectrum of cold dark matter*, *Phys. Rev. D* **71** (2005) 103520 [astro-ph/0504112] [INSPIRE].

[34] E. Bertschinger, *The Effects of Cold Dark Matter Decoupling and Pair Annihilation on Cosmological Perturbations*, *Phys. Rev. D* **74** (2006) 063509 [astro-ph/0607319] [INSPIRE].

[35] J. Silk, *Cosmic black body radiation and galaxy formation*, *Astrophys. J.* **151** (1968) 459 [INSPIRE].

[36] W. Hu and N. Sugiyama, *Small scale cosmological perturbations: An Analytic approach*, *Astrophys. J.* **471** (1996) 542 [astro-ph/9510117] [INSPIRE].

[37] A.M. Green and B.J. Kavanagh, *Primordial Black Holes as a dark matter candidate*, *J. Phys. G* **48** (2021) 043001 [arXiv:2007.10722] [INSPIRE].

[38] K. Ando, K. Inomata and M. Kawasaki, *Primordial black holes and uncertainties in the choice of the window function*, *Phys. Rev. D* **97** (2018) 103528 [arXiv:1802.06393] [INSPIRE].

[39] I. Musco, *Threshold for primordial black holes: Dependence on the shape of the cosmological perturbations*, *Phys. Rev. D* **100** (2019) 123524 [arXiv:1809.02127] [INSPIRE].

[40] M.W. Choptuik, *Universality and scaling in gravitational collapse of a massless scalar field*, *Phys. Rev. Lett.* **70** (1993) 9 [INSPIRE].

[41] J.C. Niemeyer and K. Jedamzik, *Near-critical gravitational collapse and the initial mass function of primordial black holes*, *Phys. Rev. Lett.* **80** (1998) 5481 [astro-ph/9709072] [INSPIRE].

[42] I. Musco, J.C. Miller and A.G. Polnarev, *Primordial black hole formation in the radiative era: Investigation of the critical nature of the collapse*, *Class. Quant. Grav.* **26** (2009) 235001 [arXiv:0811.1452] [INSPIRE].

[43] B. Carr, K. Kohri, Y. Sendouda and J. Yokoyama, *Constraints on primordial black holes*, *Rept. Prog. Phys.* **84** (2021) 116902 [arXiv:2002.12778] [INSPIRE].

[44] B. Carr and F. Kühnel, *Primordial black holes as dark matter candidates*, *SciPost Phys. Lect. Notes* **48** (2022) 1.

[45] M.Y. Khlopov and A.G. Polnarev, *Primordial black holes as a cosmological test of grand unification*, *Phys. Lett. B* **97** (1980) 383 [INSPIRE].

[46] T. Harada et al., *Primordial black hole formation in the matter-dominated phase of the Universe*, *Astrophys. J.* **833** (2016) 61 [arXiv:1609.01588] [INSPIRE].

[47] G. Rein, A.D. Rendall and J. Schaeffer, *Critical collapse of collisionless matter: A Numerical investigation*, *Phys. Rev. D* **58** (1998) 044007 [gr-qc/9804040] [INSPIRE].

[48] C. Gundlach and J.M. Martin-Garcia, *Critical phenomena in gravitational collapse*, *Living Rev. Rel.* **10** (2007) 5 [arXiv:0711.4620] [INSPIRE].

[49] I. Musco and J.C. Miller, *Primordial black hole formation in the early universe: critical behaviour and self-similarity*, *Class. Quant. Grav.* **30** (2013) 145009 [arXiv:1201.2379] [INSPIRE].

[50] B. Carr et al., *Primordial black hole constraints for extended mass functions*, *Phys. Rev. D* **96** (2017) 023514 [arXiv:1705.05567] [INSPIRE].

JHEP06(2023)029

[51] G. Domènech, *Scalar Induced Gravitational Waves Review*, *Universe* **7** (2021) 398 [arXiv:2109.01398] [INSPIRE].

[52] V.K. Oikonomou, *$f(R)$-Gravity Generated Post-Inflationary Eras and Their Effect on Primordial Gravitational Waves*, *Annalen Phys.* **534** (2022) 2200134 [arXiv:2205.15405] [INSPIRE].

[53] K. Kohri and T. Terada, *Semianalytic calculation of gravitational wave spectrum nonlinearly induced from primordial curvature perturbations*, *Phys. Rev. D* **97** (2018) 123532 [arXiv:1804.08577] [INSPIRE].

[54] K. Schmitz, *New Sensitivity Curves for Gravitational-Wave Signals from Cosmological Phase Transitions*, *JHEP* **01** (2021) 097 [arXiv:2002.04615] [INSPIRE].

[55] D. Baumann, P.J. Steinhardt, K. Takahashi and K. Ichiki, *Gravitational Wave Spectrum Induced by Primordial Scalar Perturbations*, *Phys. Rev. D* **76** (2007) 084019 [hep-th/0703290] [INSPIRE].

[56] H. Assadullahi and D. Wands, *Gravitational waves from an early matter era*, *Phys. Rev. D* **79** (2009) 083511 [arXiv:0901.0989] [INSPIRE].

[57] K. Inomata, K. Kohri, T. Nakama and T. Terada, *Enhancement of Gravitational Waves Induced by Scalar Perturbations due to a Sudden Transition from an Early Matter Era to the Radiation Era*, *Phys. Rev. D* **100** (2019) 043532 [arXiv:1904.12879] [INSPIRE].

[58] K. Inomata, K. Kohri, T. Nakama and T. Terada, *Gravitational Waves Induced by Scalar Perturbations during a Gradual Transition from an Early Matter Era to the Radiation Era*, *JCAP* **10** (2019) 071 [arXiv:1904.12878] [INSPIRE].

[59] M. Braglia and S. Kuroyanagi, *Probing prerecombination physics by the cross-correlation of stochastic gravitational waves and CMB anisotropies*, *Phys. Rev. D* **104** (2021) 123547 [arXiv:2106.03786] [INSPIRE].

[60] D. Alonso et al., *Noise angular power spectrum of gravitational wave background experiments*, *Phys. Rev. D* **101** (2020) 124048 [arXiv:2005.03001] [INSPIRE].

[61] G. Cusin, I. Dvorkin, C. Pitrou and J.-P. Uzan, *Stochastic gravitational wave background anisotropies in the mHz band: astrophysical dependencies*, *Mon. Not. Roy. Astron. Soc.* **493** (2020) L1 [arXiv:1904.07757] [INSPIRE].

[62] C. Caprini, R. Durrer and G. Servant, *The stochastic gravitational wave background from turbulence and magnetic fields generated by a first-order phase transition*, *JCAP* **12** (2009) 024 [arXiv:0909.0622] [INSPIRE].

[63] P. Binetruy, A. Bohe, C. Caprini and J.-F. Dufaux, *Cosmological Backgrounds of Gravitational Waves and eLISA/NGO: Phase Transitions, Cosmic Strings and Other Sources*, *JCAP* **06** (2012) 027 [arXiv:1201.0983] [INSPIRE].

JHEP06(2023)029